

Detection of Cyclopropenylidene on Titan with ALMA

CONOR A. NIXON,¹ ALEXANDER E. THELEN,^{2,1,*} MARTIN A. CORDINER,^{3,1} ZBIGNIEW KISIEL,⁴
 STEVEN B. CHARNLEY,¹ EDWARD M. MOLTER,⁵ JOSEPH SERIGANO,⁶ PATRICK G. J. IRWIN,⁷
 NICHOLAS A. TEANBY,⁸ AND YI-JEHNG KUAN^{9,10}

¹*Solar System Exploration Division, NASA Goddard Space Flight Center, Greenbelt, MD 20771, USA.*

²*Universities Space Research Association, Columbia, MD 21046, USA*

³*Catholic University of America, Washington, DC 20064, USA*

⁴*Institute of Physics, Polish Academy of Sciences, Al. Lotników 32/46, 02-668 Warszawa, Poland.*

⁵*Department of Astronomy, University of California, Berkeley, CA 94720, USA.*

⁶*Department of Earth and Planetary Sciences, Johns Hopkins University, Baltimore, MD 21218, USA.*

⁷*Atmospheric, Oceanic, and Planetary Physics, Clarendon Laboratory, University of Oxford, Parks Road, Oxford, OX1 3PU, UK.*

⁸*School of Earth Sciences, University of Bristol, Wills Memorial Building, Queens Road, Bristol, BS8 1RJ, UK.*

⁹*Department of Earth Sciences, National Taiwan Normal University, Taipei 116, Taiwan, ROC.*

¹⁰*Institute of Astronomy and Astrophysics, Academia Sinica, Taipei 106, Taiwan, ROC.*

(Received 22 April 2020; Revised 14 August 2020; Accepted 7 September 2020)

Submitted to The Astronomical Journal

ABSTRACT

We report the first detection on Titan of the small cyclic molecule cyclopropenylidene (c-C₃H₂) from high sensitivity spectroscopic observations made with the Atacama Large Millimeter/sub-millimeter Array (ALMA). Multiple lines of cyclopropenylidene were detected in two separate datasets: \sim 251 GHz in 2016 (Band 6) and \sim 352 GHz

in 2017 (Band 7). Modeling of these emissions indicates abundances of 0.50 ± 0.14 ppb (2016) and 0.28 ± 0.08 (2017) for a 350-km step model, which may either signify a decrease in abundance, or a mean value of 0.33 ± 0.07 ppb. Inferred column abundances are $3\text{--}5 \times 10^{12} \text{ cm}^{-2}$ in 2016 and $1\text{--}2 \times 10^{12} \text{ cm}^{-2}$ in 2017, similar to photochemical model predictions. Previously the C_3H_3^+ ion has been measured in Titan’s ionosphere by Cassini’s Ion and Neutral Mass Spectrometer (INMS), but the neutral (unprotonated) species has not been detected until now, and aromatic versus aliphatic structure could not be determined by the INMS. Our work therefore represents the first unambiguous detection of cyclopropenylidene, the second known cyclic molecule in Titan’s atmosphere along with benzene (C_6H_6) and the first time this molecule has been detected in a planetary atmosphere. We also searched for the N-heterocycle molecules pyridine and pyrimidine finding non-detections in both cases, and determining $2\text{-}\sigma$ upper limits of 1.15 ppb (*c*- $\text{C}_5\text{H}_5\text{N}$) and 0.85 ppb (*c*- $\text{C}_4\text{H}_4\text{N}_2$) for uniform abundances above 300 km. These new results on cyclic molecules provide fresh constraints on photochemical pathways in Titan’s atmosphere, and will require new modeling and experimental work to fully understand the implications for complex molecule formation.

Keywords: TBD

1. INTRODUCTION

Saturn’s moon Titan exhibits the most complex chemistry of any known planetary atmosphere other than the Earth. The reducing chemical environment, composed primarily of methane and nitrogen gases (Niemann et al. 2010), produces a rich array of organic molecules when activated by solar UV photons or Saturn magnetospheric electrons (Vuitton et al. 2019). Many of these daughter species are hydrocarbons (C_xH_y) or nitriles ($\text{C}_x\text{H}_y(\text{CN})_z$), however several oxygen compounds have also been detected (CO , CO_2 , H_2O), apparently due to an influx of external OH and O^+ from Enceladus (Hörst

* NASA Post-Doctoral Program Fellow

et al. 2008), and several other light gases including H_2 (from methane destruction), and the noble gases Ar and Ne.

Prior to the Cassini mission, most of our knowledge about Titan's atmospheric composition had come from remote sensing spectroscopy. While CH_4 and N_2 were detected at short wavelengths (Kuiper 1944; Broadfoot et al. 1981), most other gases were first seen in the infrared. These include the detections of C_2H_6 , C_2H_2 , C_2H_4 and CO using ground-based telescopes (Gillett et al. 1973; Gillett 1975; Lutz et al. 1983); the Voyager 1 IRIS (Infrared Interferometer-Spectrometer) detections of H_2 , C_3H_4 , C_3H_8 , C_4H_2 , HCN , HC_3N , C_2N_2 and CO_2 (Hanel et al. 1981; Maguire et al. 1981; Kunde et al. 1981; Samuelson et al. 1981; Samuelson et al. 1983); as well as later detections with ISO (Infrared Space Observatory) of H_2O and C_6H_6 (Coustenis et al. 1998, 2003). A notable exception was the detection of CH_3CN by Bezdard et al. (1992) at sub-millimeter wavelengths using the IRAM 30 m telescope at Pico Veleta.

This paradigm changed substantially with the Cassini-Huygens mission, which carried mass spectrometers on both the orbiter and the probe (Niemann et al. 2002; Young et al. 2004; Waite et al. 2004), able to sample the composition of Titan's atmosphere *in situ* for the first time. Modeling of these mass spectra revealed a plethora of ion and neutral species (Waite et al. 2005; Hartle et al. 2006; Vuitton et al. 2007, 2009; Cui et al. 2009; Bell et al. 2010a,b; Westlake et al. 2011), although in many cases exact molecular identification remained elusive, due to the inability of mass spectra alone to elucidate molecular structure. One new positive identification was made in the infrared using Cassini's CIRS instrument (Composite Infrared Spectrometer, Flasar et al. 2004), of propene (C_3H_6 , Nixon et al. 2013b). Shortly after the end of the Cassini mission, a further infrared detection was made using TEXES (the Texas Echelon-cross-Echelle Spectrograph) (Lacy et al. 2002) at NASA's Infrared Telescope Facility (IRTF): namely propadiene (CH_2CCH_2 , Lombardo et al. 2019), an isomer of propyne (C_3H_4).

The newest tool for probing Titan's atmospheric composition has been ALMA (the Atacama Large Millimeter/submillimeter Array: Baars 2002; Lellouch 2007), a powerful interferometer array that started science observations in 2011. At millimeter (mm) and submillimeter (sub-mm) wavelengths

rotational transitions of molecules are accessible, which have proved vital for probing the chemistry of astrophysical objects such as dense molecular clouds. Using early data from ALMA two further nitrile (cyanide) species were soon conclusively identified in Titan’s atmosphere: propionitrile (ethyl cyanide, C_2H_5CN , [Cordiner et al. 2015](#)) and acrylonitrile (vinyl cyanide, C_2H_3CN , [Palmer et al. 2017](#)), as well as many isotopologues of previously detected species including CO, HCN, HC_3N , CH_3CN and CH_4 ([Serigano et al. 2016](#); [Molter et al. 2016](#); [Palmer et al. 2017](#); [Cordiner et al. 2018](#); [Thelen et al. 2019a](#); [Iino et al. 2020](#)).

Besides making new chemical detections, observations of Titan from Cassini and ALMA have mapped the spatial and temporal evolution of the gas distributions, revealing complex structure such as polar jets, and seasonal changes of unexpected rapidity: see [Bézard et al. \(2014\)](#); [Hörst \(2017\)](#) for detailed reviews. In parallel with observations, photochemical modeling of Titan’s atmosphere has also progressed rapidly to explain the observed gas abundance distributions, and to make predictions for target species likely to be detectable. See for example recent work by [Krasnopolsky \(2009, 2010, 2012\)](#); [Hébrard et al. \(2013\)](#); [Krasnopolsky \(2014\)](#); [Dobrijevic et al. \(2014\)](#); [Loison et al. \(2015\)](#); [Willacy et al. \(2016\)](#); [Vuitton et al. \(2019\)](#).

In 2016 and 2017 we conducted high sensitivity observations with ALMA, with the goal of searching for new molecules in Titan’s atmosphere, including the N-heterocyclic molecules pyridine ($c-C_5H_5N$) and pyrimidine ($c-C_4H_4N_2$). N-heterocycles have a strong importance to astrobiology since these form the backbone rings for the nucleobases of DNA and RNA. Neither of these molecules were detected, and upper limits on their abundances determined instead. However, we did make a first detection on Titan of cyclopropenylidene, a small cyclic hydrocarbon molecule that has previously been detected in astrophysical sources but not in a planetary atmosphere.

This paper is organized as follows. In Section 2 we describe the observations and data reduction, and in Section 3 the data modeling process. In Section 4 we show the results, followed by a discussion in Section 5 and conclusions in Section 6.

2. OBSERVATIONS

Observations of Titan were completed during March 2–4 2016 in Band 6 (ALMA Project Code 2015.1.00423.S) and on May 8th and 16th 2017 in Band 7 (ALMA Project Code 2016.A.00014.S), see Table 1. In addition, part of a third dataset was used to obtain a CO J=2→1 observation of Titan in 2016 for retrieval of the disk-averaged temperature profile. In this independent dataset (ALMA 2015.1.00512.S, observed April 1st 2016) Titan was observed as a flux calibration target for an astrophysical investigation. Details of spectral windows (Spw) analyzed in this paper are given in Table 2.

For dataset 2015.1.00423.S the data were provided in calibrated form (bandpass, phase and flux calibrated), and subsequently post-processed using the Common Astronomy Software Applications (CASA) package Version 4.7.2-REL (r39762, March 8th 2017) to provide rest-velocity correction (`cvel`) and ephemeris update (`fixplanets`). Lastly the data were concatenated and then deconvolved (‘cleaned’) in CASA using the Högbom algorithm, with a cell size of $0.1''$ and a threshold of 10 mJy, and a final restoring beam size of $0.87'' \times 0.72''$

For the 2016 CO dataset (ALMA 2015.1.00512.S) the data were reduced in CASA Version 5.6.1-8 using the ALMA pipeline script prepared by the Joint ALMA Observatory staff, with the exception of the removal of the `hifa_fluxcalflag` task so that Titan’s atmospheric CO J=2→1 emission line at 230538 GHz was not flagged out. Data were deconvolved with the CASA `clean` task, using the Högbom algorithm with an image size = 128×128 pixels, where pixels were set to $0.2'' \times 0.2''$. The resulting synthesized beam had FWHM (Full Width to Half Maximum) = $0.92'' \times 0.81''$, comparable to Titan’s angular size at the time of observing.

The data reduction of the 2017 data (2016.A.00014.S) has already been described in [Cordiner et al. \(2019\)](#). In addition, the bandpass solution interval was increased to 10 channels (2.44 MHz) to further improve the S/N and aid in the detection of weak spectral lines (Yamaki et al., 2012).

Disk-averaged spectra from all observations were extracted from an integrated region defined by a circular pixel mask set to contain 90% of Titan’s continuum flux, as in [Lai et al. \(2017\)](#).

3. MODELING

Table 1. Details of ALMA Observations Of Titan

Date	Start (UT)	End (UT)	t * (mins)	Δv † (km s ⁻¹)	Δf ‡ (MHz)	Beam Size	Position Angle	Angular Diameter (")	Sub-Earth Latitude
<i>Project Code 2015.1.00423.S</i>									
02-Mar-2016	09:44	10:57	43	-28.37	24.13	0.87"×0.75"	89.145°	0.71	26.28
02-Mar-2016	11:03	12:14	43	-28.34	24.01	0.91"×0.73"	95.155°	0.71	26.28
04-Mar-2016	09:43	10:55	43	-32.18	27.37	0.87"×0.64"	79.815°	0.71	26.28
<i>Project Code 2015.1.00512.S</i>									
01-Apr-2016	08:22	08:24	2	-22.32	17.12	0.92"×0.81"	-83.247°	0.74	26.24
<i>Project Code 2016.A.00014.S</i>									
08-May-2017	08:49	09:07	18	-19.28	22.24	0.18"×0.15"	-80.950°	0.77	26.41
16-May-2017	05:34	07:12	98	-13.61	15.97	0.28"×0.19"	-73.549°	0.77	26.48

* Time spent on source.

† Topocentric velocity (negative = approaching).

‡ Frequency doppler shift (positive = blue-shifted).

Modeling was accomplished using the NEMESIS program (Irwin et al. 2008), which has previously been successfully applied to model ALMA spectra of Titan (e.g. Cordiner et al. 2015; Molter et al. 2016; Serigano et al. 2016; Palmer et al. 2017; Lai et al. 2017; Teanby et al. 2018; Thelen et al. 2018, 2019a,b). The NEMESIS fitting algorithm uses a Bayesian optimal estimation technique as described by Rodgers (2000), which seeks to minimize a ‘cost function’ similar to a χ^2 figure of merit, which penalizes the solution according to the square deviation of both the solution vector from the original *a priori* state, and also the model spectrum from the data. Marquart-Levenberg minimization is used to descend a downhill trajectory of the cost function until satisfactory convergence is reached (solution changing by <0.1%). ALMA spectra were rescaled to radiance units before being input to NEMESIS, and then modeled using a weighted average of spectra calculated at 35 emission angles from disk center to 1200 km altitude (3775 km radius), as described in Teanby et al. (2013), Appendix A.

Table 2. Details of observation spectral windows

Spw	Freq. Range (MHz)	Δf^\dagger (MHz)	n_{channels}	Molecule	f_0 (MHz)	Transition
<i>Project Code 2015.1.00423.S</i>						
0	249570–250050	0.244	1920	c-C ₄ H ₄ N ₂	249820	$J''=39$, ^b R-band
1	251260–251740	0.244	1920	c-C ₅ H ₅ N	251510	$J''=41$, ^a R-band
2	261900–262380	0.244	1920	c-C ₄ H ₄ N ₂	262150	$J''=41$, ^b R-band
3	263090–263570	0.244	1920	c-C ₅ H ₅ N	263340	$J''=43$, ^a R-band
<i>Project Code 2015.1.00512.S</i>						
4	230322 - 230791	0.244	1920	CO	230538	$J = 2 \rightarrow 1$
<i>Project Code 2016.A.00014.S</i>						
5	344212–346085	0.977	1920	CO	345796	$J = 3 \rightarrow 2$
6	351281–352219	0.244	3840	C ₂ H ₃ CN	—	multiple

[†]Channel spacing: spectral resolution is twice the channel spacing.

Spectral line data for most molecules were taken from the CDMS catalog (Müller et al. 2001, 2005, <https://cdms.astro.uni-koeln.de>), which is a compilation of transition information from the published literature. These include: HCN (Ahrens et al. 2002; Fuchs et al. 2004; Cazzoli & Puzzarini 2005; Maiwald et al. 2000), CO (Winnewisser et al. 1997; Goorvitch 1994), CH₃CN (Kukolich et al. 1973; Kukolich 1982; Boucher et al. 1977; Cazzoli & Puzzarini 2006), C₂H₃CN (Müller et al. 2008), c-C₄H₄N₂ (Kisiel et al. 1999) and c-C₃H₂ (Bogey et al. 1986; Vrtilik et al. 1987; Lovas 1992), including their isotopes. The rotational spectrum of c-C₅H₅N was calculated by refitting the primary spectroscopic data from Heineking et al. (1986); Wlodarczak et al. (1988). For C₂H₅CN, we used a new, more complete spectral line list that included not only rotations in the ground vibrational state, but also in the first three vibrational states as described in Kisiel et al. (2020).

Collision-induced opacity for relevant molecular pairs was computed using published formalisms and publicly-available FORTRAN codes as follows: N₂–N₂ (Borysow, A. & Frommhold, L. 1986a); N₂–CH₄ (Borysow, A. & Tang, C. 1993); CH₄–CH₄ (Borysow, A. & Frommhold, L. 1987); N₂–H₂

(Borysow, A. & Frommhold, L. 1986b); CH₄-H₂ (Borysow, A. & Frommhold, L. 1986c); H₂-H₂ (Borysow, A. 1991).

3.1. *Temperature Retrievals*

Firstly, the spectral lines of CO (Spw 4 & 5) were fitted using a model that allowed continuous variation of the temperature profile between 100–500 km, while CO was fixed at a constant mixing fraction of 49.6 ppm as determined by Serigano et al. (2016). The *a priori* temperature profile was constructed by interpolating measurements from the Huygens Atmospheric Structure Instrument (HASI) and Cassini radio science observations to Titan’s sub-observer latitude ($\sim 26^\circ$) below 100 km (Fulchignoni et al. 2005; Schinder et al. 2012), and disk-averaged retrieval results from 2015 ALMA observations of Titan (Thelen et al. 2018) were used at altitudes >100 km. Temperature *a priori* errors were set to 5 K in all atmospheric layers (0–1200 km), which allowed NEMESIS to obtain a fit to the data while limiting artificial vertical structure (ill-conditioning) in the retrieved temperature profile. Different frequency offsets from the line center sounded to different atmospheric depths (altitudes, or pressure levels), as shown by the contribution functions in Fig. 1. The *a priori* and final retrieved temperature profiles are also indicated.

3.2. *Spectral windows 1 and 6: Discovery of Cyclopropenylidene*

Next Spw 1¹ was modeled to fit visible lines of known molecules: C₂H₅CN and C₂H₃CN. The temperature profile was fixed at the earlier retrieved profile from Spw 4 for 2016. Various gas profile types were investigated for the nitriles, adjusting the profiles to achieve best fits.

We first tried using minimalist ‘step’ functions (uniform volume mixing ratio above a fixed pressure level, and zero below) for the vertical distribution of each gas. From previous experience (e.g. Cordiner et al. 2015; Lai et al. 2017) we found that these worked well for trace (low abundance) nitriles in the ALMA spectrum where there is little information that can be obtained about the vertical profile. For C₂H₃CN we adopted a step altitude at 300 km. For C₂H₅CN, there was sufficient sensitivity to the

¹ Window 0 was not included in this study. This region contains isotopic lines of CH₃C¹⁵N, the analysis of which will be reported elsewhere. See also recent work on this isotopologue by Iino et al. (2020)

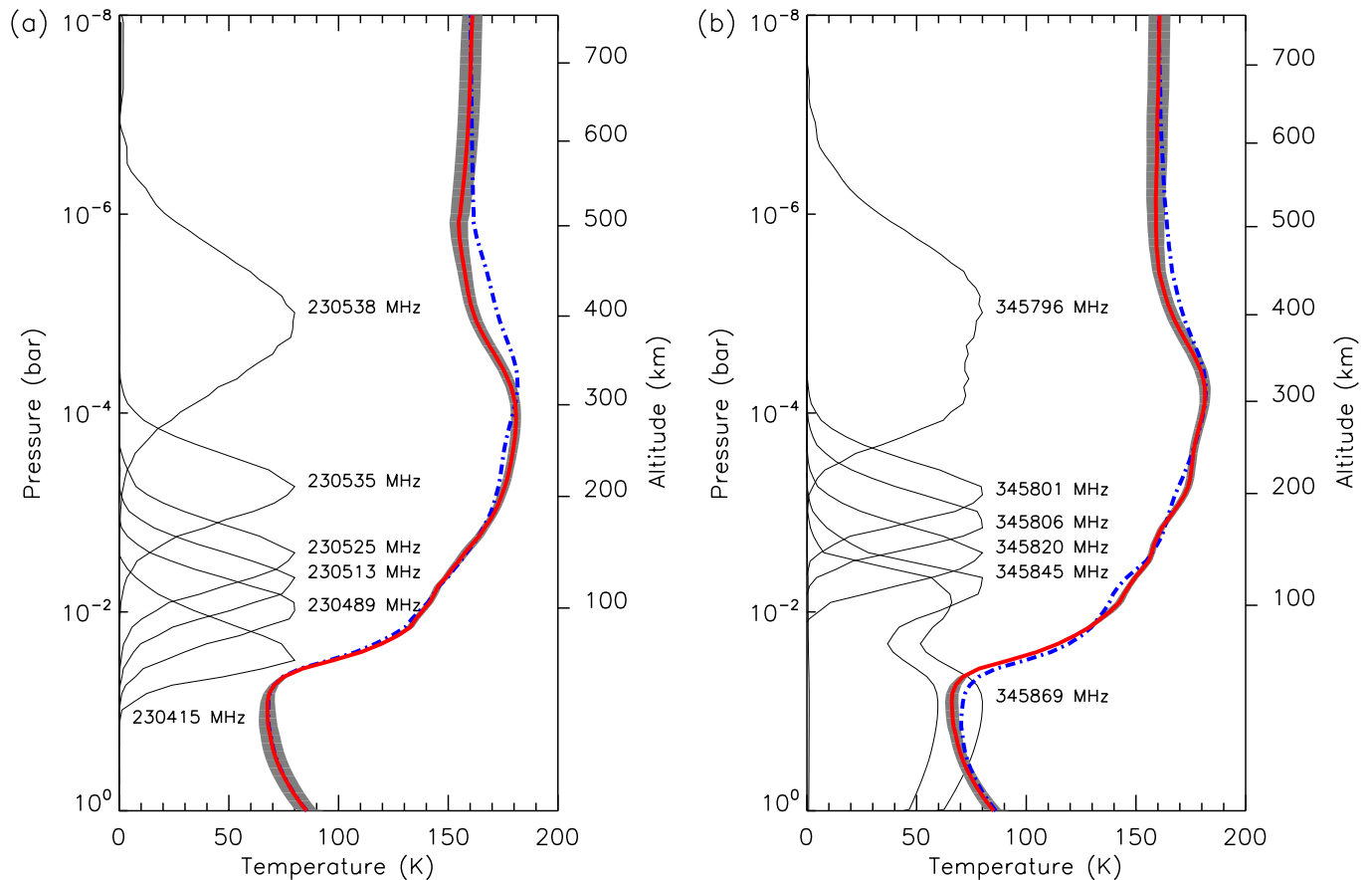


Figure 1. Temperature retrievals for (a) CO 2→1 in 2016 and (b) CO 3→2 in 2017. Blue dot-dash lines: *a priori* temperature profiles. Red solid line: retrieved profiles, with shaded (grey) retrieval error indicated. Normalized contribution functions at different frequencies are also shown (thin solid black lines).

altitude of the step to affect the quality of the fit, which was determined from Spw 1 and thereafter fixed at 250 km (see Appendix A). Initial fitting is shown in Fig. 2.

Having fitted the features of the known nitrile gases as well as possible, we proceeded to try adding additional gases to the model in an attempt to detect any weak lines due to a new species, including *i*-butanenitrile and *n*-butanenitrile (C_3H_7CN), propynenitrile (cyanodiacetylene, HC_5N) and others, using lines from the JPL catalog (Pickett et al. 1998, <https://spec.jpl.nasa.gov>). In both Spw 1 and 6, we found a significant improvement to the model fit after introducing the gas $c\text{-}C_3H_2$ (cyclopropenylidene) using spectroscopic lines from CDMS originally determined by Bogey et al. (1986); Vrtilek et al. (1987) with a trial step function model with a step at 300 km, or higher.

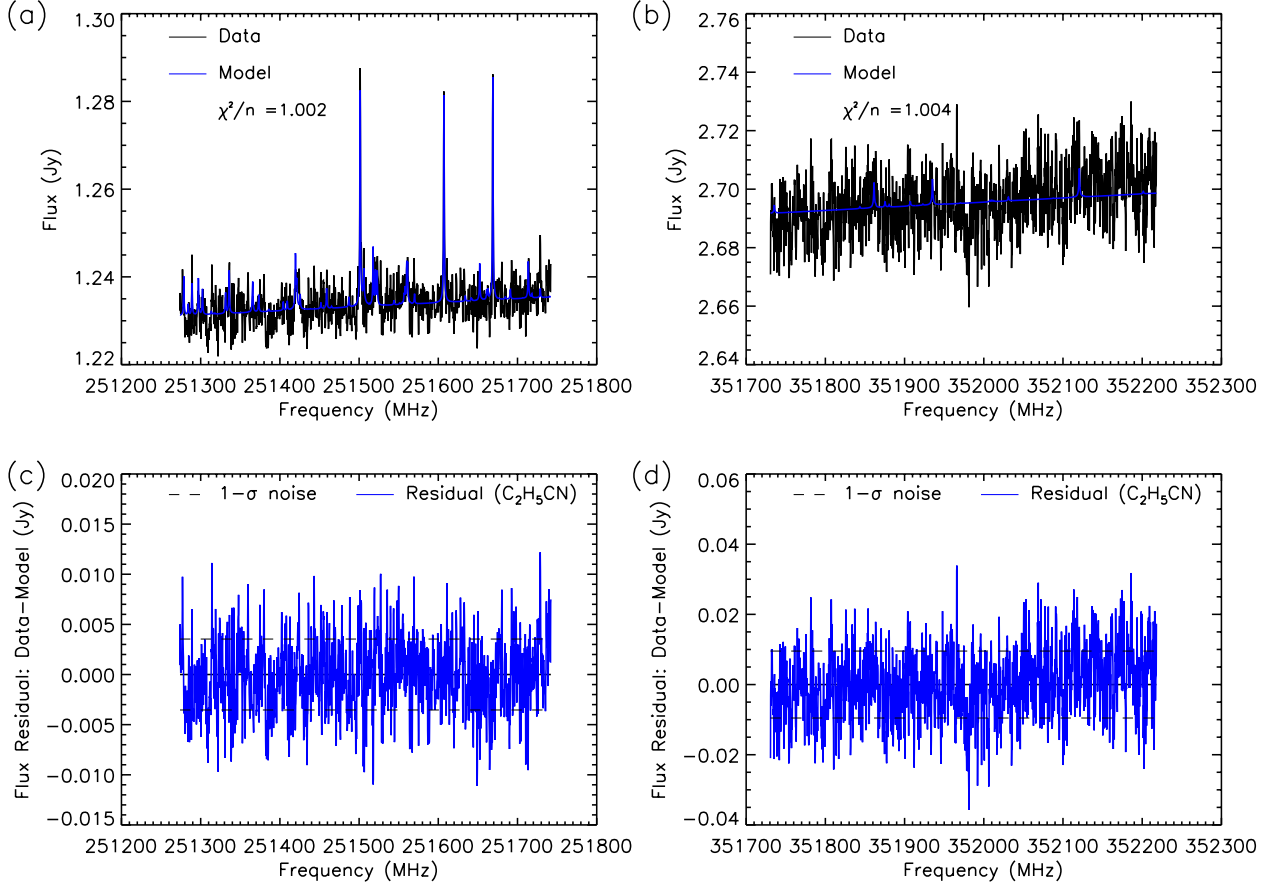


Figure 2. Best fit models for Spw 1 (a) and Spw 6 (b) using previously known gases only. Gas profiles were step function models for C_2H_5CN (250 km) and C_2H_3CN (300 km). Residuals after fitting are shown in panels (c) and (d). Frequencies have been corrected to rest velocity frame.

In Spw 1 two significant lines were detected at 251314.3 MHz (blend of $7_{0,7} \rightarrow 6_{1,6}$ and $7_{1,7} \rightarrow 6_{0,6}$ transitions) and 251527.3 MHz ($6_{2,5} \rightarrow 5_{1,4}$), as shown in Fig. 3. We note that these two emissions are the strongest expected spectral features of $c\text{-}C_3H_2$ in Spw 1, and show close to the expected proportions of relative intensities.

Similarly, in Spw 6, despite the noise level being higher in ALMA Band 7 than in Band 6 (Spw 1), we made two further detections of lines of $c\text{-}C_3H_2$: 351781.6 MHz (blend of the $10_{1,10} \rightarrow 9_{0,9}$ and $10_{0,10} \rightarrow 9_{1,9}$ doublet), 351965.9 MHz (blend of $9_{1,8} \rightarrow 8_{2,7}$ and $9_{2,8} \rightarrow 8_{1,7}$ doublet), see Fig. 4.

To further test the detection of $c\text{-}C_3H_2$, we calculated a $\Delta\chi^2$ curve for different amounts of the gas in a forward model, using a step function at 350 km. In this case, $\chi^2 = \sum_{\nu} [(S_{\nu} - I_{\nu})/\sigma_{\nu}]^2$ is a metric

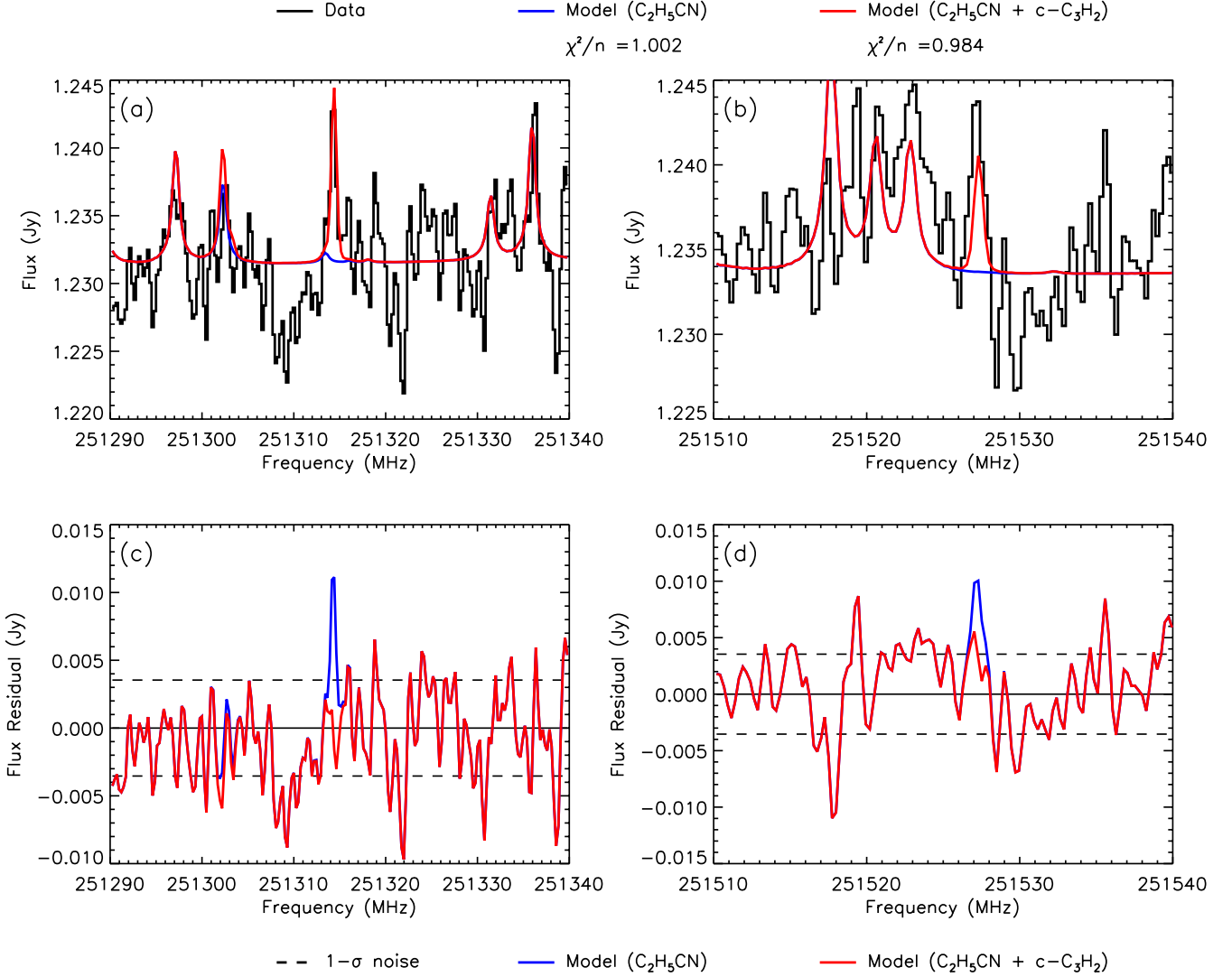


Figure 3. Modeling of Spw 1 showing expanded scale of regions where detected $c\text{-C}_3\text{H}_2$ lines are present: blend of $7_{0,7} \rightarrow 6_{1,6}$ and $7_{1,7} \rightarrow 6_{0,6}$ transitions at 251314.3 MHz, and $6_{2,5} \rightarrow 5_{1,4}$ single transition at 251527.3 MHz. Blue: $\text{C}_2\text{H}_5\text{CN}$ model only. Red: model with $\text{C}_2\text{H}_5\text{CN}$ and $c\text{-C}_3\text{H}_2$. Frequencies have been corrected to rest velocity frame.

of spectral goodness-of-fit, where S_ν is the data spectrum, I_ν is the model spectrum, and σ_ν is the spectral noise estimate. However, note that this is not the same definition as the more commonly used ‘reduced chi-square’ metric: χ^2/n , where n is the number of spectral points minus the number of degrees of freedom (model parameters). In this case therefore a good fit occurs when $\chi^2 \simeq n$ (rather than $\chi^2/n \simeq 1$). We then define $\Delta\chi^2$ as the improvement to χ^2 for various model trial abundances:

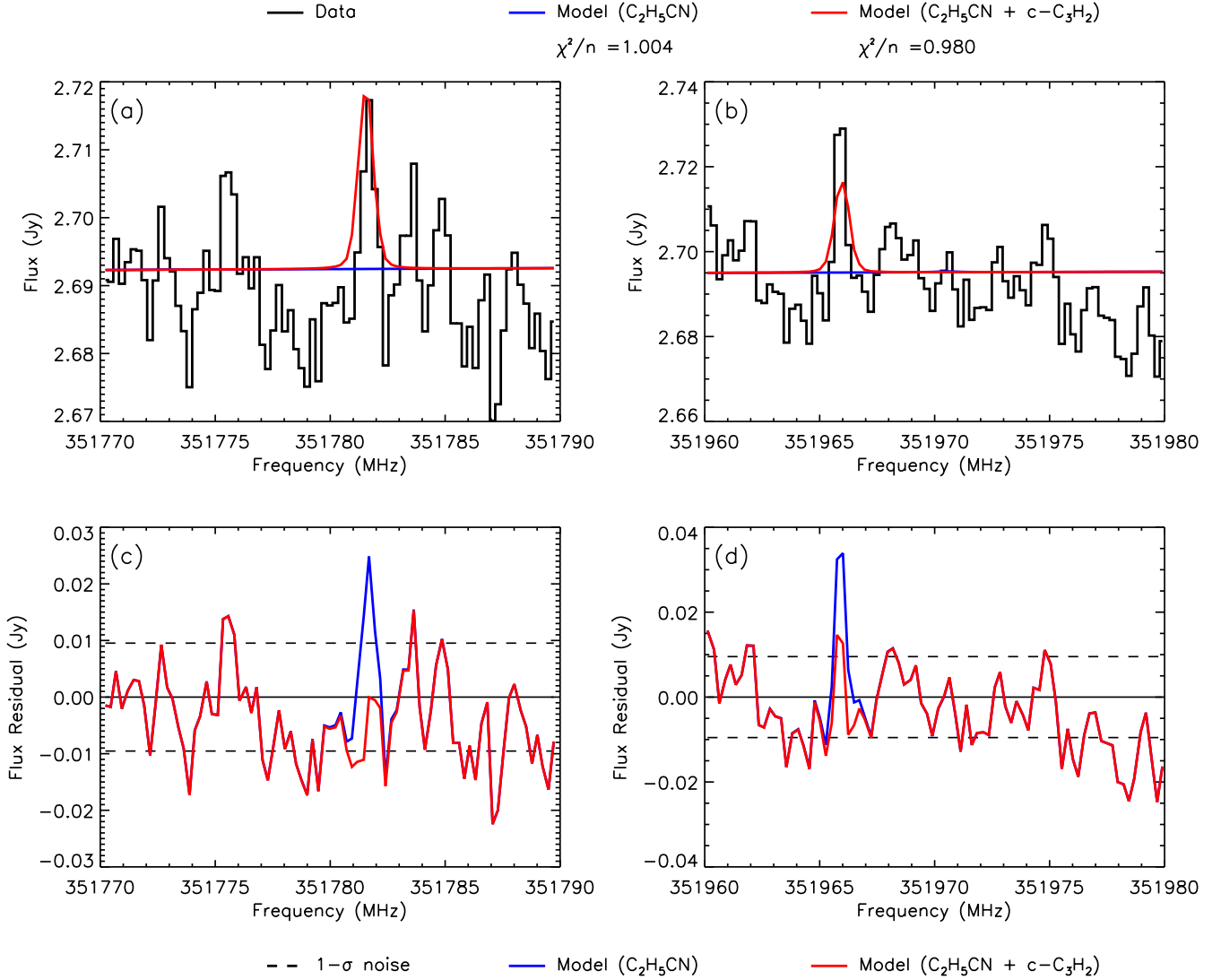


Figure 4. Modeling of Spw 6 showing expanded scale of regions where detected $c-C_3H_2$ lines are present: blend of $10_{1,10} \rightarrow 9_{0,9}$ and $10_{0,10} \rightarrow 9_{1,9}$ doublet at 351781.6 MHz, and blend of $9_{1,8} \rightarrow 8_{2,7}$ and $9_{2,8} \rightarrow 8_{1,7}$ doublet at 351965.9 MHz. Blue: C_2H_5CN model only. Red: model with C_2H_5CN and $c-C_3H_2$. Frequencies have been corrected to rest velocity frame.

$\Delta\chi^2 = \chi_q^2 - \chi_0^2$, where χ_0^2 denotes the best-fit model in absence of the trial gas, and χ_q^2 is the same metric when an amount q of the trial gas is present in the model (Teunby et al. 2009; Nixon et al. 2010, 2013a; Teunby et al. 2018). An improved fit results in a $\Delta\chi^2$ that decreases below zero, and worsening fit results in $\Delta\chi^2$ that increases above zero.

Results are shown in Fig. 5. A strong minimum is seen for a volume mixing ratio $q = 0.5$ ppb in Band 6, with $\Delta\chi^2$ reaching -21.24 indicating a $\sqrt{21.24} = 4.6 \sigma$ significance to the result. For Band 7, a minimum is reached at mole fraction $q = 0.25$ ppb with $\Delta\chi^2 = -18.69$ (4.3σ). Both results are significant, although the mixing ratio determined in each case is somewhat different (but consistent within error bars, as shown later in Section 4). The combined significance of the detection is 6.3σ .

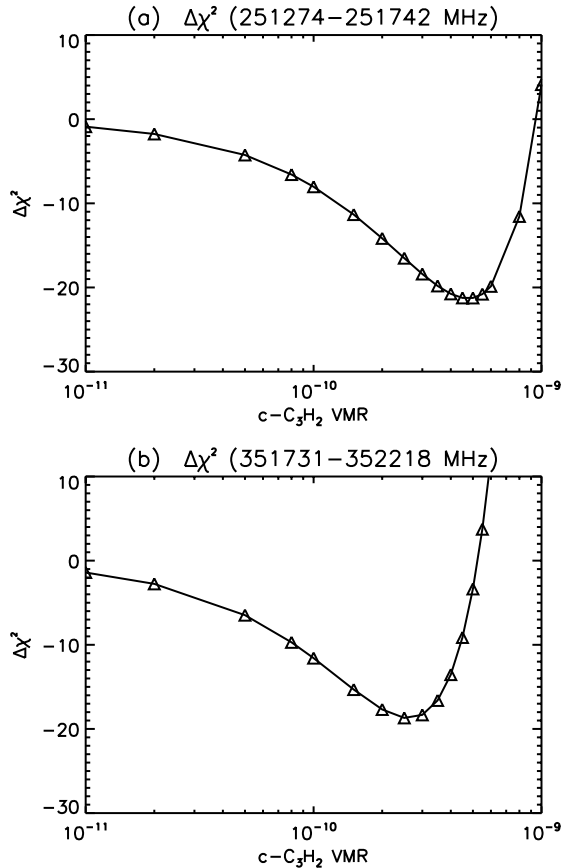


Figure 5. Change in χ^2 ($\Delta\chi^2$) for various trial abundances of $c\text{-C}_3\text{H}_2$ using a 350 km step model. (a) Band 6, showing a $4.6\text{-}\sigma$ minimum at a volume mixing ratio (VMR) of 0.50 ppb. (a) Band 7, showing a $4.3\text{-}\sigma$ minimum at a volume mixing ratio (VMR) of 0.25 ppb.

Retrieved abundances for $c\text{-C}_3\text{H}_2$ with various profiles are described in Section 4.

3.3. Spectral windows 2 and 3: Search for pyridine and pyrimidine

Fitting for Spw 2 & 3 was accomplished by initially using the retrieved temperature profile from Spw 4, and also scaling a 250-km step model for $\text{C}_2\text{H}_5\text{CN}$ and 300-km step model for $\text{C}_2\text{H}_3\text{CN}$. In

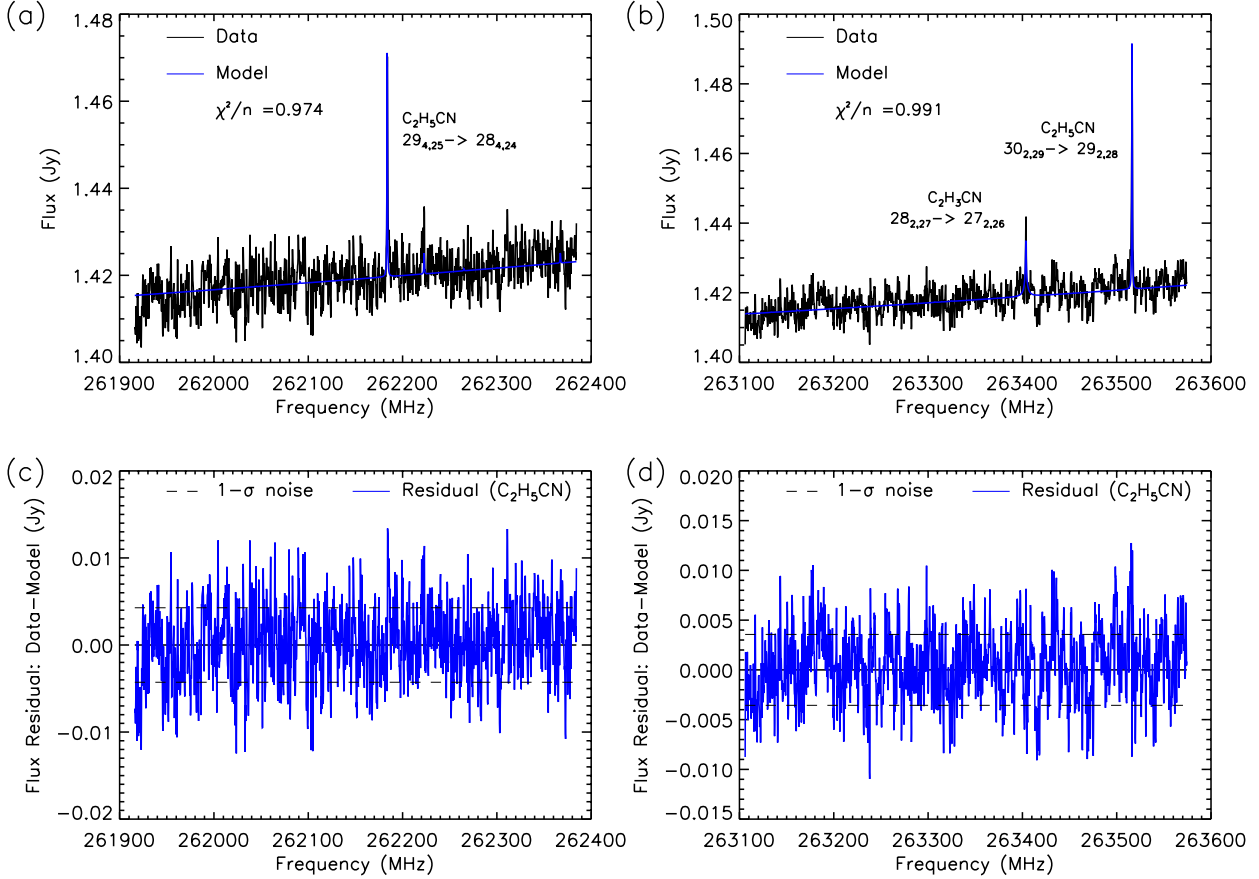


Figure 6. Best fit models for Spw 2 and 3. In Spw 2 (panel (a), and residual in panel (c)) we see a single strong line of C₂H₅CN at 262183.8 (29_{4,25} → 28_{4,24}), while in Spw 3 (panel (b), and residual in panel (d)) we detect C₂H₃CN at 263403.7 MHz (28_{2,27} → 27_{2,26}), and C₂H₅CN at 263516.2 MHz (30_{2,29} → 29_{2,28}). Frequencies have been corrected to rest velocity frame.

in addition, we included HCN which contributed a continuum slope in these windows due to the wings of the strong 3 → 2 line at 265886 MHz whose line center lies outside the bandpass. Then, 300-km step model profiles models for c-C₅H₅N (Spw 2) and c-C₄H₄N₂ (Spw 3) were introduced, but resulted in no significant improvement to the fit as measured by a reduced χ^2 test. Instead, upper limits for c-C₅H₅N and c-C₄H₄N₂ were determined instead (see Section 4.) The final fit for these spectral windows is shown in Fig. 6.

4. RESULTS

4.1. Retrieval errors

The propagation of errors in the retrieval process follows the formalism described in Irwin et al. (2008), and further elaborated in Section 3.5 of Nixon et al. (2008) (hereafter N08). This includes a combination of *a priori* and measurement error (Eq. 1 of N08), with the error from the earlier temperature propagated as additional measurement error (Eq. 2 of N08). In addition, we needed to make a further error allowance for apodization, which reduces independent information in the spectrum. Due to the Hanning apodization applied during the Fourier Transform, neighboring spectral channels become correlated, and the signal-to-noise in our retrieval will be overestimated by a factor equal to the square root of the number of channels per resolution element - two channels per resolution element for Hanning apodization. At the same time, there is a small gain of 1.095 from averaging information across two successive correlated channels², so the final error bars are increased by a factor $\sqrt{2}/1.095 = 1.291$. This factor has also been applied to correspondingly reduce the detection significances (σ levels) throughout the paper.

4.2. Cyclopropenylidene

We initially fitted the c-C₃H₂ emissions with a step function model, where the gas abundance was zero below a ‘step’ altitude and a uniform value above. The overall profile was then scaled to achieve a best fit. The effect of changing the altitude of the step was also explored, since lower steps increased pressure broadening of the lines that became greater than the observed line widths.

We also investigated a more realistic gas profile, with an abundance decreasing downwards to a condensation altitude, by using a four-parameter gradient model. This model was defined by two (p, q) (pressure, mixing ratio) co-ordinates defining a straight-line, logarithmically decreasing VMR between (p_u, q_u) (upper point) and (p_l, q_l) (lower point). Above p_u the VMR was assumed constant at q_u and below p_l the VMR dropped to zero. The upper pressure level was set to be $p_u = (5.0 \pm 2.0) \times 10^{-11}$ bar, or approximately 1100 km, the altitude of the INMS measurements of the C₃H₂H⁺ (protonated) ion. The initial value for the abundance at this altitude was set to be $q_u = (3.4 \pm 1.0) \times 10^{-6}$ in line with the INMS ion measurements (Vuitton et al. 2007). The initial

² ALMA technical notes: <https://help.almascience.org/index.php?/Knowledgebase/Article/View/29>

value for the lower point was set to be: $p_l = (1.0 \pm 0.5) \times 10^{-4}$ bar, $q_l = (2.0 \pm 1.9) \times 10^{-9}$, a pressure level corresponding to approximately 300 km, and allowing a lenient variation of abundance.

Scaled step function solutions for *c*-C₃H₂ from Window 1 (Band 6) and Window 6 (Band 7) are shown in Fig. 7, along with best fit gradient model profiles. Numerical results are given in Table 3. Retrievals for cyclopropenylidene showed low sensitivity to the altitude of the step, with a weak minimum at 300–400 km. The resulting abundances and columns were slightly different in 2016 and 2017. For a step function of 350 km we obtained a VMR of 0.50 ± 0.14 ppb and column abundance of 3.5×10^{12} cm⁻² in 2016, but somewhat lower VMR (0.28 ± 0.08) and column abundance (1.5×10^{12}) in 2017. This implies either (a) that the global abundance had decreased from 2016 to 2017, or, (b) if the real abundance was constant, then a mean value of 0.33 ± 0.07 ppb for the 350 km step profile.

Table 3. Retrieved column abundances and volume mixing ratios (VMRs) at 600 km for different *c*-C₃H₂ models.

Band	Species	Model	χ^2/n	VMR (ppb @ 600 km)	Col. Abund. (molecule cm ⁻²)
6	<i>c</i> -C ₃ H ₂	Gradient model	0.9843	3.788	2.649×10^{12}
6	<i>c</i> -C ₃ H ₂	400 km step	0.9839	1.012 ± 0.386	2.824×10^{12}
6	<i>c</i> -C ₃ H ₂	350 km step	0.9838	0.495 ± 0.142	3.487×10^{12}
6	<i>c</i> -C ₃ H ₂	300 km step	0.9841	0.278 ± 0.054	4.875×10^{12}
7	<i>c</i> -C ₃ H ₂	Gradient model	0.9791	1.867	1.197×10^{12}
7	<i>c</i> -C ₃ H ₂	400 km step	0.9789	0.537 ± 0.223	1.175×10^{12}
7	<i>c</i> -C ₃ H ₂	350 km step	0.9800	0.279 ± 0.084	1.541×10^{12}
7	<i>c</i> -C ₃ H ₂	300 km step	0.9829	0.122 ± 0.031	1.702×10^{12}

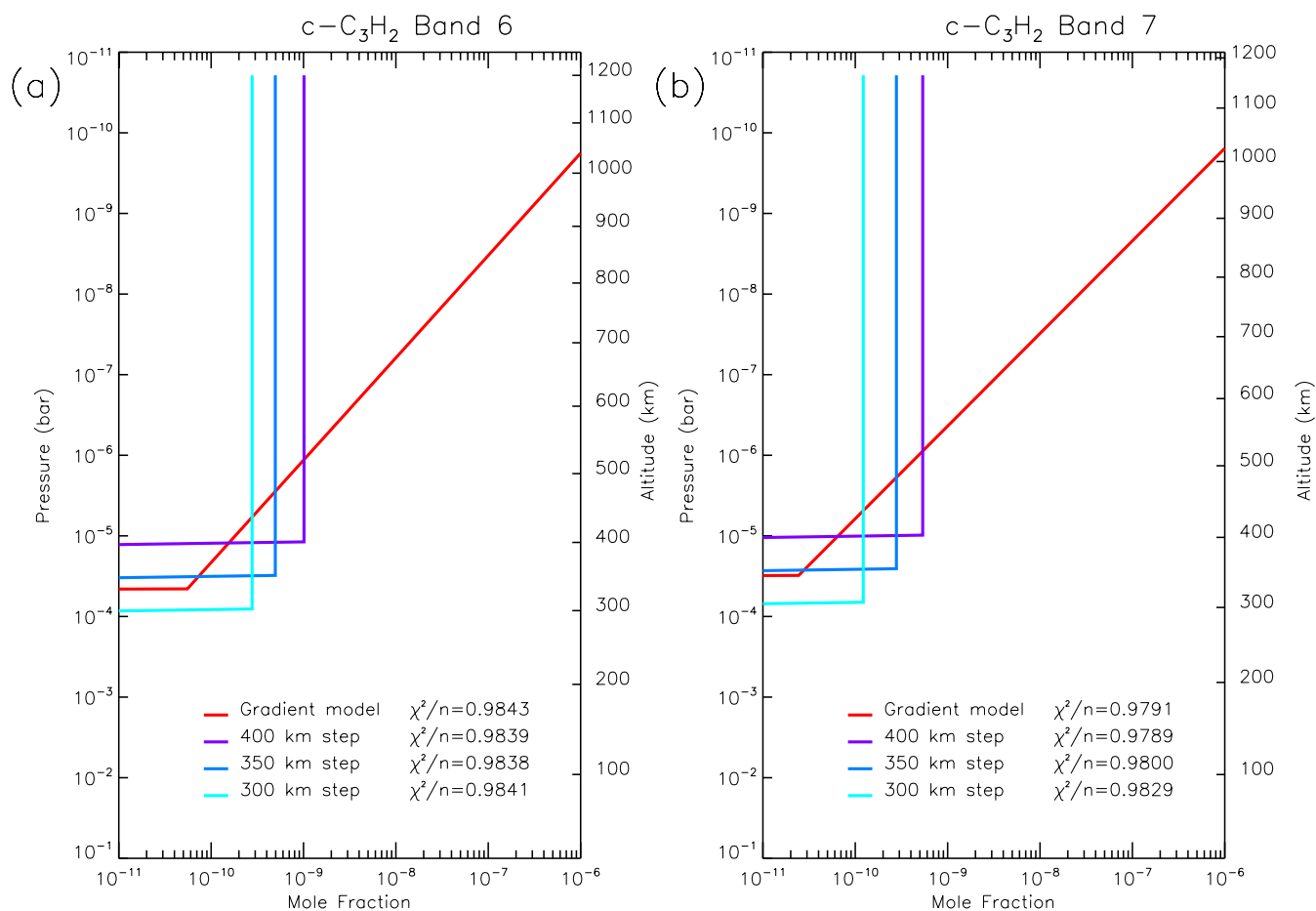


Figure 7. Retrieved profiles of $c\text{-C}_3\text{H}_2$ for different models. (a) Band 6 data, 2016. (b) Band 7 data, 2017.

Retrieved parameters for the gradient model retrievals in 2016 and 2017 are shown in Table 4, along with parameters for a weighted mean profile of both years.

4.3. Pyridine and pyrimidine

Upper limits for $c\text{-C}_5\text{H}_5\text{N}$ and $c\text{-C}_4\text{H}_4\text{N}_2$ were determined using the $\Delta\chi^2$ method outlined for $c\text{-C}_3\text{H}_2$ in Section 3.2. In this case, the 1, 2 and 3- σ upper limits are indicated at the trial abundances where the $\Delta\chi^2$ reaches +1, +4, and +9 respectively (Nixon et al. 2012). Results are shown in Fig. 8 and Table 5. A shallow minimum was detected for $c\text{-C}_5\text{H}_5\text{N}$, however the spectrum does not show obvious emissions consistent with expected spectral lines, therefore we believe this to be likely due to random spectral noise (although worthy of a more sensitive follow-up observation to be sure).

Table 4. Retrieved parameters for c-C₃H₂ gradient model fits

	p_u (bar)	q_u	p_l (bar)	q_l
<i>Band 6</i>				
<i>a priori</i>	$(5.0 \pm 2.0) \times 10^{-11}$	$(3.4 \pm 1.0) \times 10^{-6}$	$(1.0 \pm 0.5) \times 10^{-4}$	$(2.0 \pm 1.9) \times 10^{-9}$
Retrieved	$(4.4 \pm 2.2) \times 10^{-11}$	$(3.1 \pm 1.2) \times 10^{-6}$	$(4.7 \pm 2.9) \times 10^{-5}$	$(5.4 \pm 3.7) \times 10^{-11}$
<i>Band 7</i>				
<i>a priori</i>	$(5.0 \pm 2.0) \times 10^{-11}$	$(3.4 \pm 1.0) \times 10^{-6}$	$(1.0 \pm 0.5) \times 10^{-4}$	$(2.0 \pm 1.9) \times 10^{-9}$
Retrieved	$(4.3 \pm 2.2) \times 10^{-11}$	$(3.1 \pm 1.2) \times 10^{-6}$	$(3.8 \pm 2.3) \times 10^{-5}$	$(2.1 \pm 1.7) \times 10^{-11}$
<i>Band 6 & 7</i>				
Combined	$(4.3 \pm 1.6) \times 10^{-11}$	$(3.1 \pm 0.8) \times 10^{-6}$	$(4.1 \pm 1.8) \times 10^{-5}$	$(2.6 \pm 1.5) \times 10^{-11}$

Table 5. Upper limits for undetected nitrogen heterocycle molecules in Titan’s atmosphere

Name	p (μ bar)	Freq. (MHz)	NEF [†] (mJy)	1- σ VMR [‡]	2- σ VMR [‡]	3- σ VMR [‡]
c-C ₄ H ₄ N ₂	0.020	262143	0.34	0.663	0.854	1.042
c-C ₅ H ₅ N	0.020	263331	0.29	1.046	1.153	1.356

[†]Noise Equivalent Flux. [‡]Volume Mixing Ratio (mole fraction) in ppb.

5. DISCUSSION

5.1. Cyclopropenylidene

The molecule cyclopropenylidene (c-C₃H₂) was discovered in the interstellar medium (ISM) by [Thaddeus et al. \(1985\)](#) through extensive laboratory and theoretical analysis to unearth the origin of several prominent, but previously unidentified lines seen on radio astronomical spectra. Following this discovery, the molecule has been found to be ubiquitous in the galaxy ([Fosse et al. 2001](#)) and easily detectable due to the relatively large dipole of 3.43(2) D ([Kanata et al. 1987](#)) caused by the unpaired electrons on the bivalent carbon atom. In addition, c-C₃H₂ is a light molecule with a small partition function, which also works in favor of detection. One of its linear isomers, propadienylidene (H₂CCC,

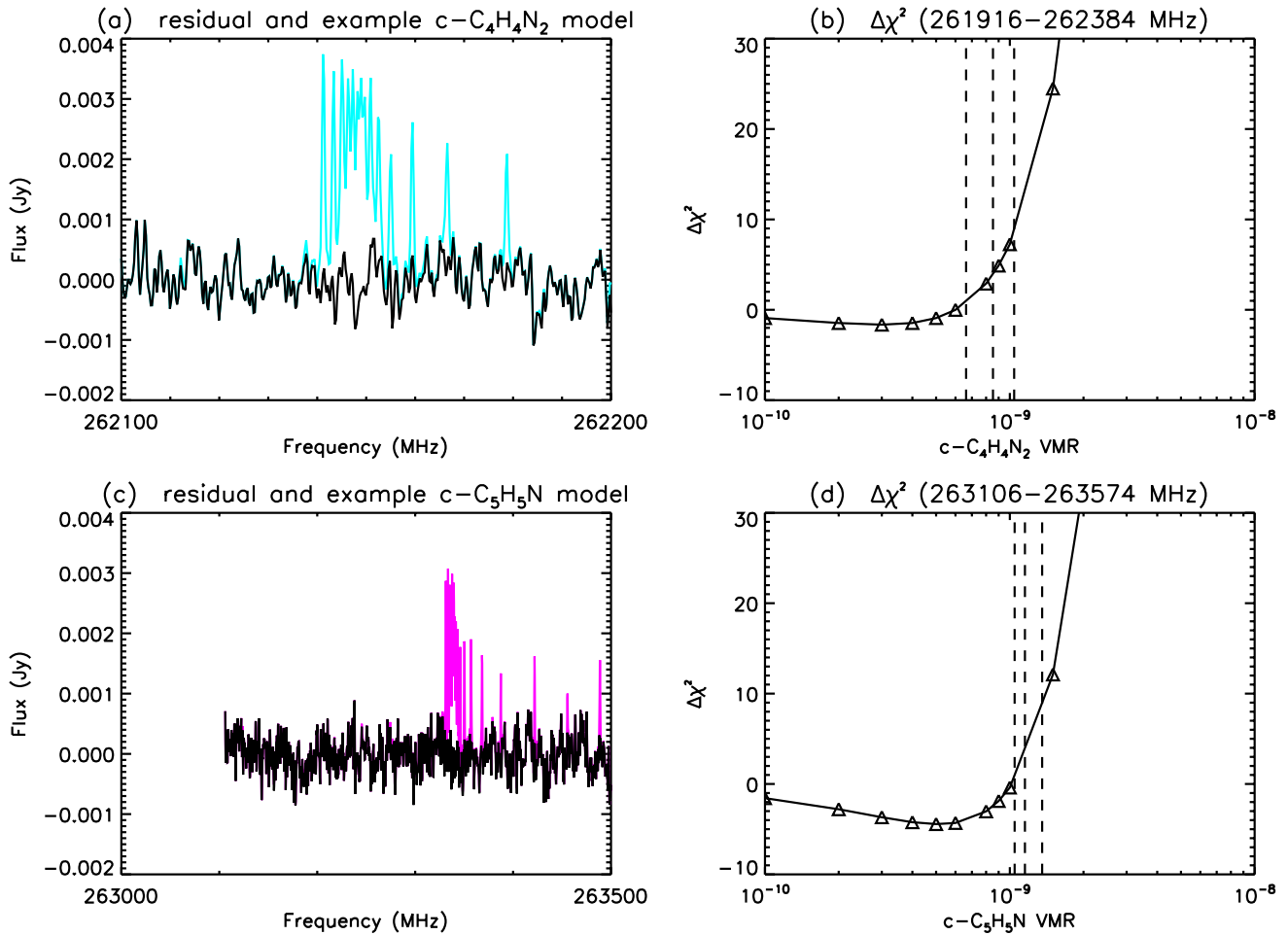


Figure 8. Upper limit determination for nitrogen heterocycle molecules. (a) Data (black) and example spectrum (cyan) for $c\text{-C}_4\text{H}_4\text{N}_2$ showing missing spectral band location. (b) $\Delta\chi^2$ curve for various trial abundances for $c\text{-C}_4\text{H}_4\text{N}_2$. (c) Data (black) and example spectrum (magenta) for $c\text{-C}_5\text{H}_5\text{N}$ showing missing spectral band location. (d) $\Delta\chi^2$ curve for various trial abundances for $c\text{-C}_5\text{H}_5\text{N}$. Vertical dashed lines on (b) and (d) indicate the 1, 2, and 3- σ upper abundance limits at $\Delta\chi^2 = +1, +4, +9$.

see Fig. 9) has since been detected in the ISM (Cernicharo et al. 1991) while propynylidene (HCCCH) has not been observed. Note that propadienylidene is higher in energy than cyclopropenylidene, and therefore metastable, so that the observed ratio of ten or more for $c\text{-C}_3\text{H}_2/\text{H}_2\text{CCC}$ is expected.

The Cassini INMS instrument measured peaks at m/z 38 and 39 in samples of Titan’s upper atmosphere that were attributed to the presence of C_3H_2^+ and various isomers of C_3H_3^+ (Vuitton et al. 2006; Vuitton et al. 2007). Although the molecular structure was not directly measurable,

modeling of the mass spectrum implied ion number densities of 0.0016 cm^{-3} (C_3H_2^+), 34 cm^{-3} ($\text{c-C}_3\text{H}_3^+$) and 1.6 cm^{-3} ($\text{l-C}_3\text{H}_3^+$) respectively. Determining the ratio of $\text{l-C}_3\text{H}_3^+/\text{c-C}_3\text{H}_3^+$ was deemed to be of major importance by [Vuitton et al. \(2007\)](#) (and the subject of laboratory investigation), since the linear propargyl ion is able to react to form heavier species, including possibly benzene ([Wilson & Atreya 2004](#)), while the cyclopropenylidene ion is essentially a terminal species, leading to $\text{c-C}_3\text{H}_2$.

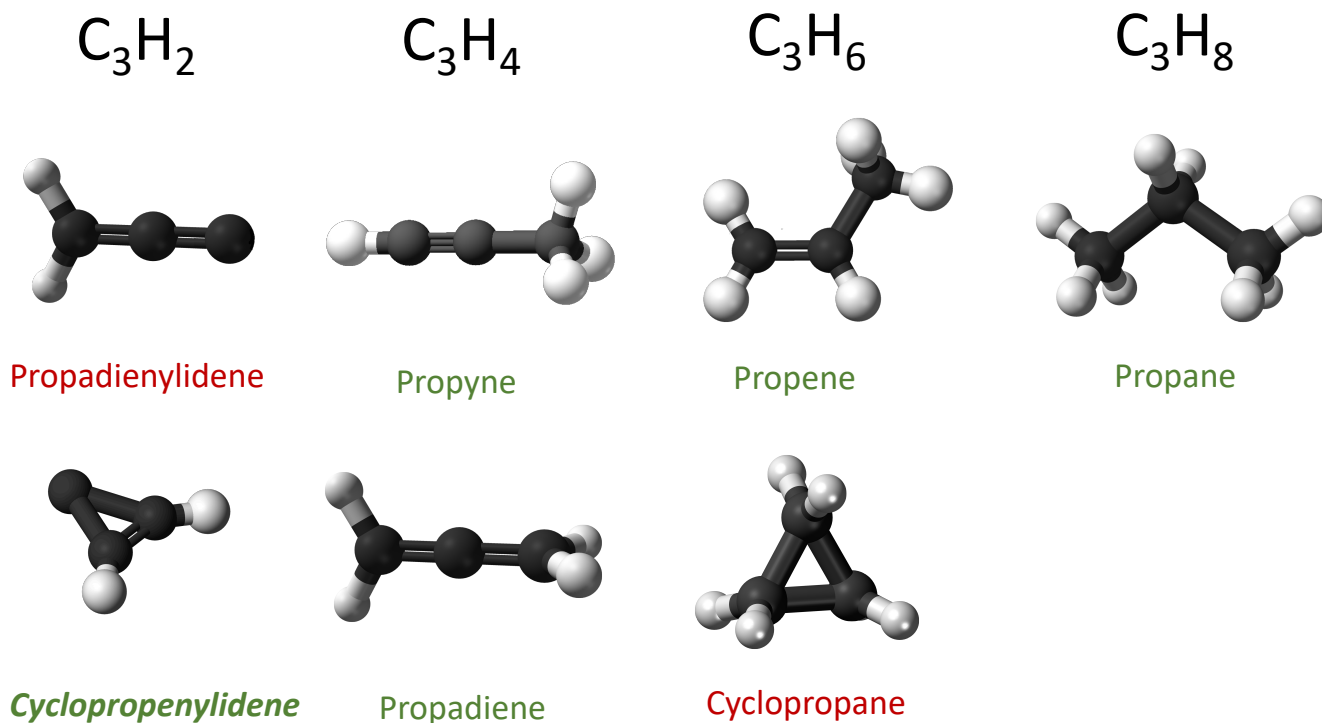
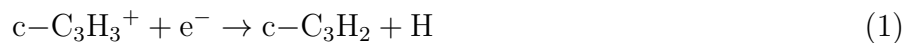


Figure 9. Structures of C_3H_x molecules. Green lettering = detected in Titan's atmosphere. Red lettering = undetected. Molecule graphics: wikimedia commons.

Various mechanisms have been proposed for the formation of $\text{c-C}_3\text{H}_2$ and it is not clear at present which mechanisms are the most important. In the original work of [Thaddeus et al. \(1985\)](#) on the ISM detection, cyclopropenylidene was produced by dissociative electron recombination of the cyclopropenylum cation, $\text{c-C}_3\text{H}_3^+$:



while $\text{c-C}_3\text{H}_3^+$ is produced from C_2H_2 in two steps. First the fast ion-molecule reaction:



followed by the slower radiative association (hydrogenation):

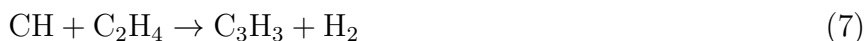


Alternatively the C_3H_3^+ ion has been proposed to be produced from acetylene via many other possible ion molecule reactions by [Vuitton et al. \(2019\)](#), for example:



[Walch \(1995\)](#); [Guadagnini et al. \(1998\)](#) investigated the reactions of $\text{CH}(X^2\Pi)$ (methylidyne) with C_2H_2 , predicting that various isomers of both C_3H_3 and C_3H_2 can result. From this point, several outcomes are possible: the products can stabilize into a less-reactive species, such as $\text{c-C}_3\text{H}_2$, or else can undergo further reactions to form heavier hydrocarbons. In particular, it was noted that both C_3H_3 and C_3H_2 can dimerize, forming benzene (C_6H_6) and *para*-benzene (C_6H_4) respectively, and therefore C_3H_3 and C_3H_2 are important stepping stones to polycyclic aromatic hydrocarbons (PAHs).

The work of [Canosa et al. \(1997\)](#) further clarified pathways to formation of C_3H_2 from reactions of the methylidyne radical (CH) with unsaturated C_2H_x hydrocarbons, such as:



In the above reactions, CH is envisaged to add to the carbon-carbon double or triple bond. C_3H_3 can be converted to C_3H_2 by hydrogen loss through photodissociation (e.g. [Hébrard et al. 2013](#)):



The C_3H radical may also result from the methyldiene insertion reactions, which can lead to C_3H_2 via several steps, first charge transfer:



followed by hydrogenation (3) and then dissociative recombination (1) as before. Subsequently, [Canosa et al. \(2007\)](#) showed that C_2 reactions may also be important, e.g.:



as used in the photochemical model of [Krasnopolsky \(2009\)](#). The branching ratios between aliphatic and aromatic pathways in many of these reactions, especially at low temperatures, are important and often poorly known.

In Fig. 10 we compare our retrieved gradient models to photochemical model predictions of [Hébrard et al. \(2013\)](#) and [Vuitton et al. \(2019\)](#). In fact, the models arrive at a column abundance rather similar to our retrieved amount of $\sim 10^{12} \text{ cm}^{-2}$. It is difficult to pronounce whether the differences in the vertical profile shape are significant or not, since we have very little constraint on this at present.

5.2. *Pyridine and pyrimidine*

The astrobiologically important species pyridine ($c\text{-}C_5H_5N$) and pyrimidine ($c\text{-}C_4H_4N_2$) are nitrogen-containing heterocyclic ring molecules resembling a benzene ring with either one or two of the C-H members replaced by a nitrogen atom. Pyrimidine in particular is of significant biological importance since it forms the backbone ring structure of several key biological molecules - specifically the nucleobases uracil (in RNA), cytosine (in RNA and DNA) and thymine (in DNA). These molecules can potentially be formed from pyrimidine after the chemical substitution of functional groups ($-NH_2$, $-CH_3$ and $=O$) in place of hydrogen, as indicated in Fig. 11. Indeed, laboratory experiments ([Nuevo et al. 2014](#)) have shown that UV irradiation of pyrimidine in the presence of H_2O , CH_4 , CH_3OH and NH_3 can form uracil and cytosine - but not the more complex thymine - a possible clue as to why thymine appears only in DNA but not RNA, and further evidence that RNA may

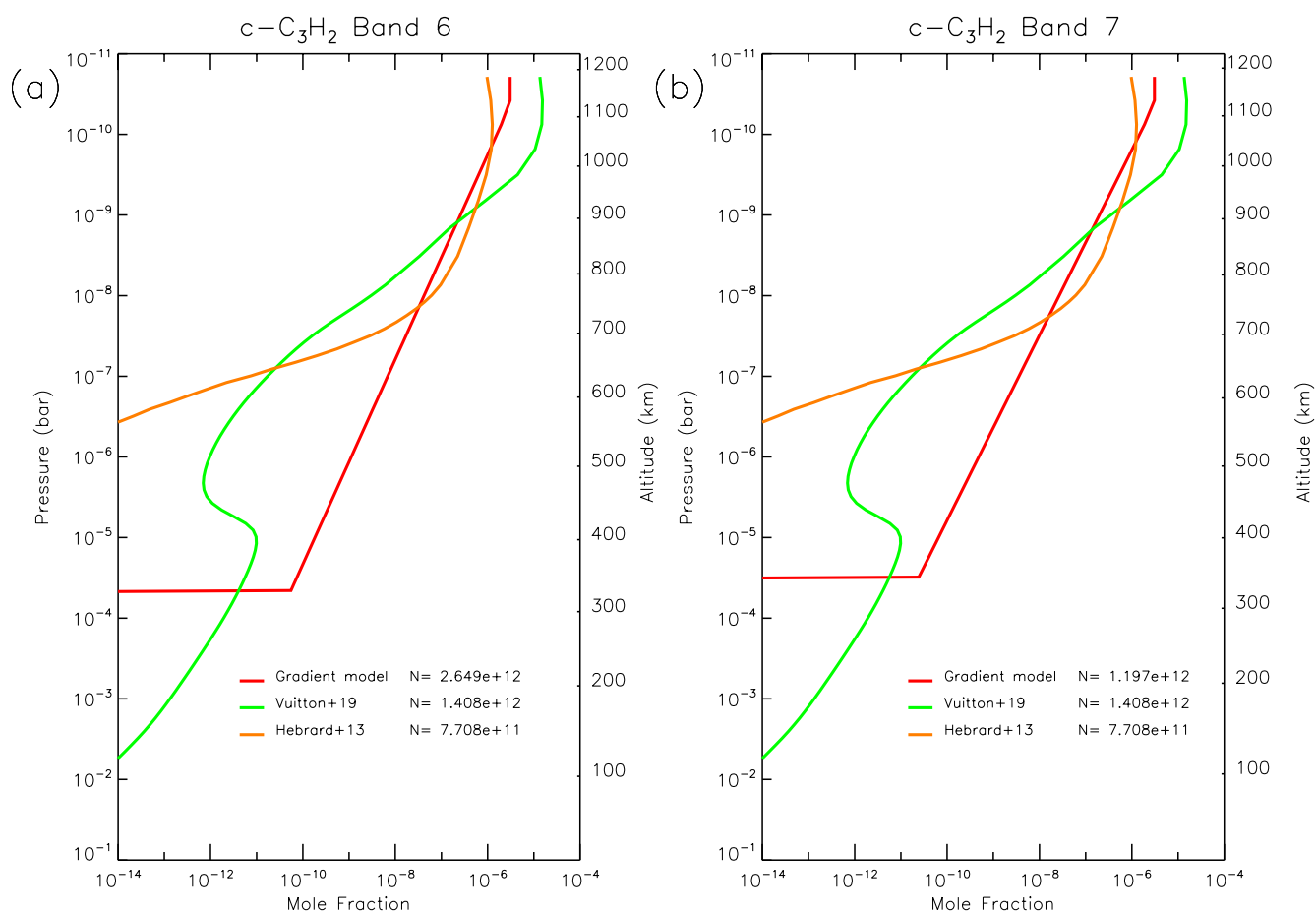


Figure 10. Retrieved gas abundance profiles for $c\text{-C}_3\text{H}_2$ in Band 6 and Band 7 using the gradient model compared to published photochemical models. Column abundances (N) are in molecule cm^{-2} .

have preceded DNA. Similar processes may be taking place in space, including the atmosphere of Titan. Indeed, laboratory simulations of Titan's atmosphere, using multiple experimental techniques such as GC-MS (gas chromatograph mass spectroscopy), pyrolysis mass spectroscopy, Raman and reflectance spectroscopy etc have been successful in positively identifying the nitrogen heterocycles (Khare et al. 1984; Ehrenfreund et al. 1995).

To date, neither pyridine nor pyrimidine have been detected in astrophysical sources, despite searches in molecular clouds (Simon & Simon 1973; Kuan et al. 2003, 2004; Cordiner et al. 2017; McGuire et al. 2018) and in the envelopes of evolved stars (Charnley et al. 2005), although pyridine and quinoline (2-membered N-heterocycle rings) derivatives have been found in meteorite samples (e.g. Stoks & Schwartz 1982; Martins 2018). Peeters et al. (2005) have shown that these molecules

Known to exist on Titan

Potentially exist in Titan's atmosphere

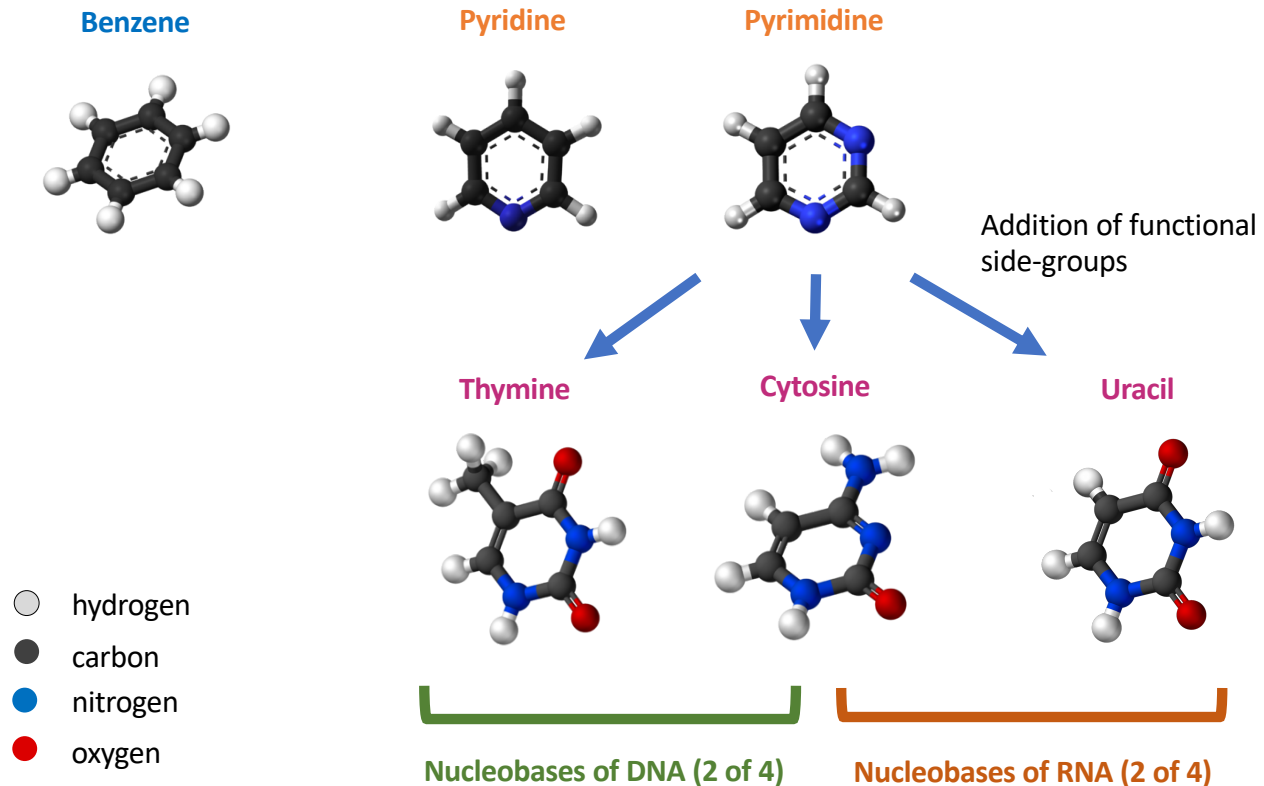
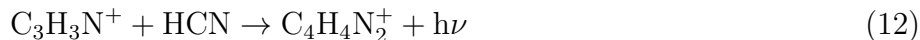


Figure 11. Importance of nitrogen heterocycle molecules such as pyridine and pyrimidine to astrobiology: detection of such species would indicate a possible route to creation of nucleobases of DNA and RNA. Individual molecule graphics from wikimedia commons.

are relatively unstable against UV irradiation compared to benzene, but could survive for 10–100s of years in dense clouds where UV flux is attenuated, and therefore potentially in Titan's thick atmosphere.

The potential presence of the nitrogen heterocyclic molecules pyridine and pyrimidine in Titan's atmosphere may be inferred from the detection of $C_5H_5NH^+$ and $C_4H_4N_2H^+$ ions in Cassini mass spectra (Vuitton et al. 2007) at m/z 80 and 81 (seen in their Fig. 2). As with the hydrocarbons, the elucidation of structure from the mass spectra alone is not possible, therefore for example protonated forms of branched acyclic molecules such as penta-2,4-dienitrile or 2-methylene-3-butenitrile could be responsible for the mass 80 peak instead.

Formation pathways for the N-heterocycles are currently quite uncertain. For example, [Fondren et al. \(2007\)](#) suggest that efficient ion-molecule association reactions with HCN could form pyridine and pyrimidine from smaller ions:



A more exotic mechanism for the formation of pyridine through ring expansion of pyrrole by methyldyne has been observed in the gas phase by [Soorkia et al. \(2010\)](#):



More recently, [Balucani et al. \(2019\)](#) has investigated a pathway to pyridine that begins with an attack on C_6H_6 by $\text{N}(^2\text{D})$, leading to a chain of unstable intermediate products that may decay to $\text{c-C}_5\text{H}_5\text{N}$.

The relative importance of these various channels is highly uncertain at the present time, leading to difficulties in incorporating these molecules into photochemical models. For example [Krasnopolsky \(2009\)](#) included just one hypothetical formation pathway for pyridine by the radical-molecule reaction:



while in [Loison et al. 2015](#)) only the aliphatic isomer $\text{C}_2\text{H}_5\text{C}_3\text{N}$ is discussed.

Our analysis indicates $2\text{-}\sigma$ upper limits of ~ 1.15 ppb and ~ 0.85 ppb for $\text{c-C}_5\text{H}_5\text{N}$ and $\text{c-C}_4\text{H}_4\text{N}_2$ respectively (constant profile above 300 km), which may in future be used to place some constraints on photochemical models as these become more sophisticated and add more detailed treatment of cyclic molecule formation.

6. CONCLUSIONS

We report the first detection of $\text{c-C}_3\text{H}_2$ (cyclopropenylidene) on Titan in two datasets: Band 6 spectra from 2016 and Band 7 data from 2017, detecting at least 2 emissions in each case. The

derived abundances are 0.50 ± 0.14 ppb in 2016 and 0.28 ± 0.08 in 2017 for a 350-km step model, which are in agreement at the margins of their $1\text{-}\sigma$ errors, or alternatively may indicate a real decrease in abundance. Derived column abundances are $3\text{--}5 \times 10^{12}$ cm^{-2} in 2016 and $1\text{--}2 \times 10^{12}$ cm^{-2} in 2017, in good agreement with photochemical models. This presence of cyclopropenylidene is of substantial significance to Titan’s atmospheric chemistry, since insertion reactions of methylidyne (CH) into C_2H_2 and other unsaturated hydrocarbons can lead to formation of C_3H_2 and C_3H_3 isomers. These in turn may be stepping stones to benzene and *para*-benzene, and larger aromatic PAH molecules.

Following preliminary evidence from Cassini mass spectra, we also searched for the N-heterocyclic molecules pyridine and pyrimidine in Titan’s atmosphere, with a null result. By modeling of ALMA spectra at 262–263 GHz we have determined $2\text{-}\sigma$ upper limits of 1.15 and 0.85 ppb for *c*- $\text{C}_5\text{H}_5\text{N}$ and *c*- $\text{C}_4\text{H}_4\text{N}_2$ respectively. We have detected ground state lines of $\text{C}_2\text{H}_3\text{CN}$ and $\text{C}_2\text{H}_5\text{CN}$ as previously seen in Titan’s atmosphere, and also vibrationally excited rotational transitions of $\text{C}_2\text{H}_5\text{CN}$. The $\text{C}_2\text{H}_5\text{CN}$ emissions are well-fitted using a 250 km ‘step’ model as noted by previous authors, and we find a best-fit abundance of 5.0 ± 0.1 ppb similar to previous work. Our modeling indicates that there is unlikely to be substantial amounts of $\text{C}_2\text{H}_5\text{CN}$ below 250 km, in contrast to existing photochemical models.

The discovery of cyclopropenylidene for the first time in a dense planetary atmosphere therefore opens up new directions for research in the chemistry of the reducing atmospheres of the outer planets, and especially PAH and haze formation.

ACKNOWLEDGMENTS

C.A.N. and M.A.C. received support for this work through NASA’s Solar System Observations (SSO) Program. C.A.N. and A.E.T. were also funded by NASA’s Astrobiology Program. M.A.C. was supported by the National Science Foundation under Grant No. AST-1616306. PGJI and NAT are funded by the UK Science and Technology Facilities Council.

This paper makes use of the following ALMA data: ADS/JAO.ALMA#2015.1.00423.S, 2015.1.00512.S, 2016.A.00014.S. ALMA is a partnership of ESO (representing its member states),

NSF (USA) and NINS (Japan), together with NRC (Canada), MOST and ASIAA (Taiwan), and KASI (Republic of Korea), in cooperation with the Republic of Chile. The Joint ALMA Observatory is operated by ESO, AUI/NRAO and NAOJ. The National Radio Astronomy Observatory is a facility of the National Science Foundation operated under cooperative agreement by Associated Universities, Inc.

APPENDIX

A. PROPIONITRILE

A.1. *Modeling*

In Spw 1, sufficiently strong lines of $\text{C}_2\text{H}_5\text{CN}$ were seen that there was noticeable pressure-induced line broadening, allowing an optimum altitude for a step function model to be determined. Fig. 12 shows the effect of changing the step function altitude for $\text{C}_2\text{H}_5\text{CN}$.

The goodness of fit for all models is compared in Table 6. The best-fit solution for $\text{C}_2\text{H}_5\text{CN}$ is a step function at 250 km with a uniform VMR of 5.0 ± 0.07 ppb and column abundance $2.2 \times 10^{14} \text{ cm}^{-2}$. A comparison of retrieved profiles can be seen in Fig. 13(a).

Table 6. Retrieved column abundances and volume mixing ratios (VMRs) at 600 km for different model types for $\text{C}_2\text{H}_5\text{CN}$.

Species	Model	χ^2/n	VMR (ppb @ 600 km)	Col. Abund (molecule cm^{-2})
$\text{C}_2\text{H}_5\text{CN}$	Gradient model	1.051	31.957	1.3475×10^{14}
$\text{C}_2\text{H}_5\text{CN}$	300 km step	1.035	8.545 ± 0.252	1.5004×10^{14}
$\text{C}_2\text{H}_5\text{CN}$	250 km step	1.002	5.040 ± 0.095	2.2378×10^{14}
$\text{C}_2\text{H}_5\text{CN}$	200 km step	1.159	2.749 ± 0.030	3.5703×10^{14}

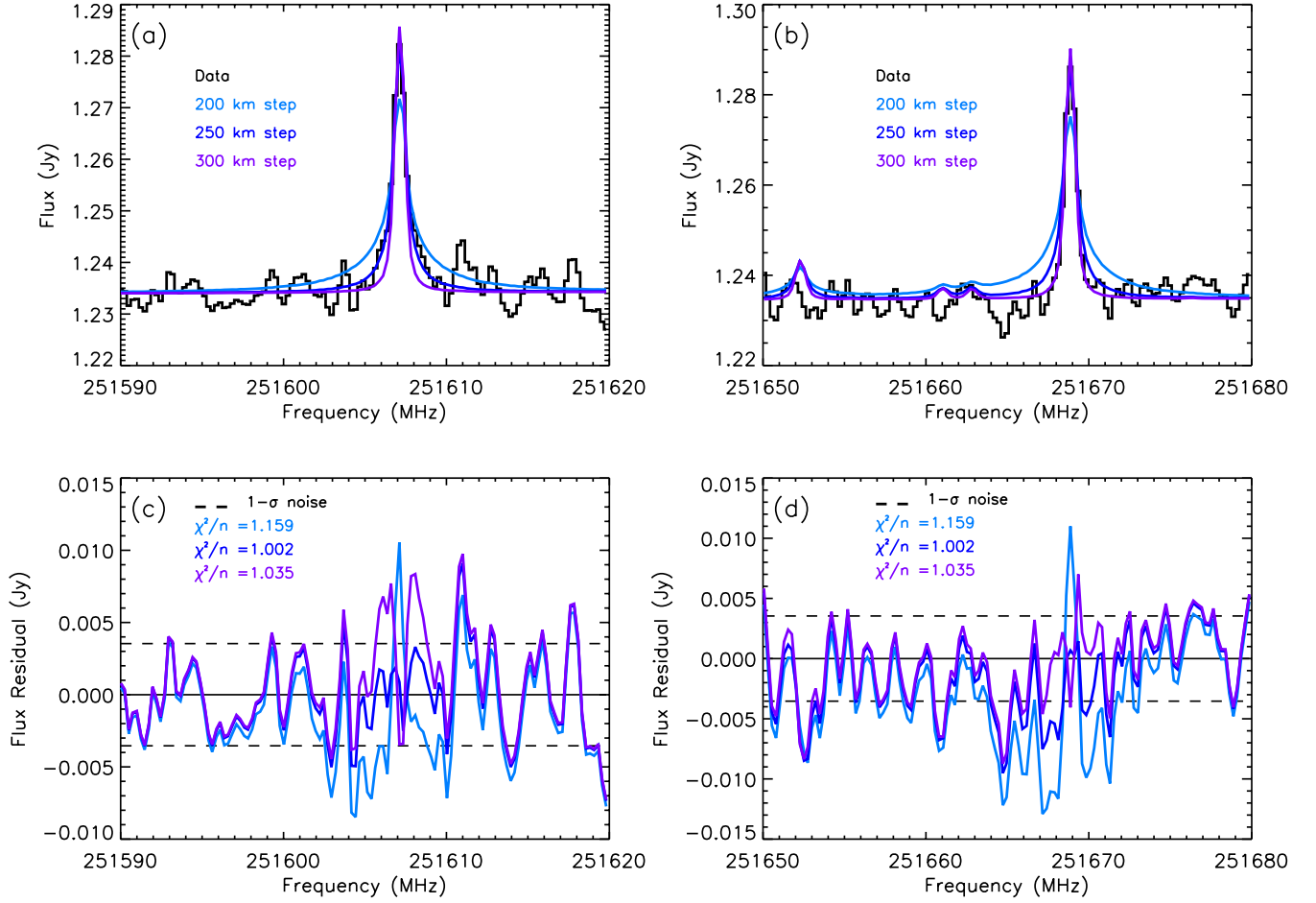


Figure 12. Spectral fitting of strong $\text{C}_2\text{H}_5\text{CN}$ lines in Spw 1 using ‘step’ models at different altitudes (panels (a) and (b)), and residual after fitting (panels (c) and (d)). Frequencies have been corrected to rest velocity frame.

Table 7. Retrieved parameters for gradient model fits

Gas		p_u (bar)	q_u	p_l (bar)	q_l
$\text{C}_2\text{H}_5\text{CN}$	<i>a priori</i>	$(5.0 \pm 2.0) \times 10^{-11}$	$(5.0 \pm 1.0) \times 10^{-7}$	$(1.0 \pm 0.5) \times 10^{-4}$	$(2.0 \pm 1.9) \times 10^{-9}$
$\text{C}_2\text{H}_5\text{CN}$	Retrieved	$(4.7 \pm 2.4) \times 10^{-11}$	$(4.8 \pm 1.3) \times 10^{-7}$	$(1.1 \pm 0.6) \times 10^{-4}$	$(4.3 \pm 0.9) \times 10^{-9}$

A gradient model was also tested, using similar initial conditions to those used for $\text{c-C}_3\text{H}_2$, as described in Section 3.2, except that the initial abundance at the 1100 km altitude was set to $q_u = (5.0 \pm 1.0) \times 10^{-7}$ in line with the INMS measurement of $\text{C}_2\text{H}_5\text{CNH}^+$. Initial and retrieved parameters for the $\text{C}_2\text{H}_5\text{CN}$ gradient model are given in Table 7.

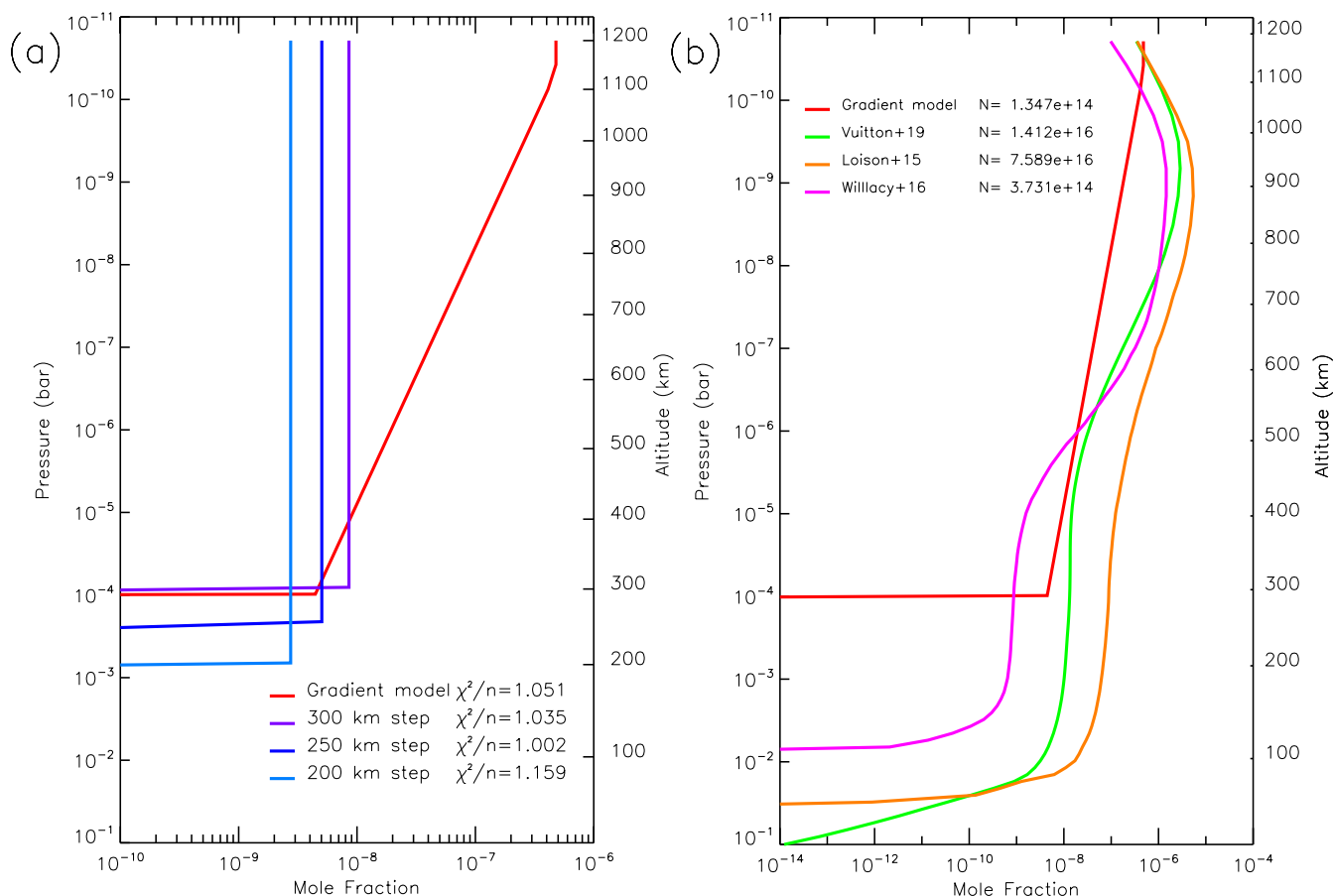


Figure 13. (a) Retrieved model profiles for C_2H_5CN . (b) Comparison between gradient model for C_2H_5CN and published photochemical model profiles.

A list of the ground-state and vibrationally excited lines detected in Spw 1 is given in Table 8.

In the next section the implications of the results for C_2H_5CN are discussed.

A.2. Discussion: C_2H_5CN

The ion $C_2H_5CNH^+$ was inferred from early Cassini INMS mass spectra of Titan's upper atmosphere (e.g. Vuitton et al. 2007), and the first identification of ethyl cyanide (propionitrile) in the neutral atmosphere was achieved using ALMA by Cordiner et al. (2015). Nitrile molecules have a large molecular dipole (~ 4.0 D for small nitriles, equivalent to 70% of an equivalent ionic bond), causing them to have strong rotational spectra. This was undoubtedly a reason why methyl cyanide (acetonitrile, CH_3CN) was first detected at sub-millimeter wavelengths (Bezard et al. 1992), and despite intensive searching has yet to be detected in the infrared (Nixon et al. 2010).

Table 8. Lines of C₂H₅CN detected in Spw 1

Species	Freq. (MHz)	Transition ^a	v^b	E_u (K)
C ₂ H ₅ CN	251271.3	30 _{6,24} -30 _{5,25}	0	240
C ₂ H ₅ CN	251278.7	28 _{18,-} 27 _{18,}	0	533
C ₂ H ₅ CN	251284.2	28 _{16,-} 27 _{16,}	2	776
C ₂ H ₅ CN	251289.1	28 _{12,-} 27 _{12,}	1	624
C ₂ H ₅ CN	251297.1	28 _{11,-} 27 _{11,}	1	600
C ₂ H ₅ CN	251302.3	28 _{13,-} 27 _{13,}	1	651
C ₂ H ₅ CN	251331.4	28 _{14,-} 27 _{14,}	1	680
C ₂ H ₅ CN	251335.9	28 _{10,-} 27 _{10,}	1	577
C ₂ H ₅ CN	251365.8	28 _{19,-} 27 _{19,}	0	573
C ₂ H ₅ CN	251373.2	28 _{15,-} 27 _{15,}	1	712
C ₂ H ₅ CN	251404.3	28 _{6,23} -27 _{6,22}	3	751
C ₂ H ₅ CN	251409.4	28 _{6,22} -27 _{6,21}	3	751
C ₂ H ₅ CN	251419.7	28 _{9,-} 27 _{9,}	1	557
C ₂ H ₅ CN	251425.6	28 _{16,-} 27 _{16,}	1	744
C ₂ H ₅ CN	251459.0	28 _{20,-} 27 _{20,}	0	616
C ₂ H ₅ CN	251487.2	28 _{17,-} 27 _{17,}	1	780
C ₂ H ₅ CN	251501.0	28 _{5,24} -27 _{5,23}	0	203
C ₂ H ₅ CN	251517.7	28 _{8,-} 27 _{8,}	1	539
C ₂ H ₅ CN	251520.6	28 _{6,23} -27 _{6,22}	2	524
C ₂ H ₅ CN	251522.9	28 _{6,22} -27 _{6,21}	2	524
C ₂ H ₅ CN	251558.1	28 _{21,-} 27 _{21,}	0	661
C ₂ H ₅ CN	251560.2	28 _{6,23} -27 _{6,22}	1	509
C ₂ H ₅ CN	251561.2	28 _{6,22} -27 _{6,21}	1	509
C ₂ H ₅ CN	251570.0	31 _{6,26} -31 _{5,27}	0	253
C ₂ H ₅ CN	251607.1	28 _{5,23} -27 _{5,22}	0	202
C ₂ H ₅ CN	251652.3	28 _{5,24} -27 _{5,23}	2	511
C ₂ H ₅ CN	251661.0	10 _{4,7} -9 _{3,6}	0	41
C ₂ H ₅ CN	251668.8	28 _{4,25} -27 _{4,24}	0	193
C ₂ H ₅ CN	251691.0	28 _{5,24} -27 _{5,23}	3	739
C ₂ H ₅ CN	251713.6	28 _{5,23} -27 _{5,22}	2	511
C ₂ H ₅ CN	251728.7	10 _{4,6} -9 _{3,7}	0	41

^a Rotational energy levels are labeled with J , K_a , K_c , and omission of K_c identifies a degenerate spectroscopic doublet in which $K_c = J - K_a$ and $K_c = J - K_a + 1$.

^b Vibrational species: 0: ground state (Brauer et al. 2009), 1: $v_{13} = 1$ (Kisiel et al. 2020), 2: $v_{21} = 1$ (Kisiel et al. 2020), 3: $v_{20} = 1$ (Daly et al. 2013).

The detection of C_2H_5CN by [Cordiner et al. \(2015\)](#) in ALMA Band 6 data at ~ 220 – 240 GHz was close to the region observed in this work, with an abundance of ~ 9 ppb (300 km step model) derived from disk-averaged observations in July 2012. Several years later, follow-up work by [Palmer et al. \(2017\)](#) also in Band 6 near 230 GHz determined a disk-average abundance of 7.2 ± 0.29 ppb for early 2014, while [Lai et al. \(2017\)](#) measured 7.37 ± 0.32 ppb from April 2015 data in Band 7 near 348 GHz. Our measurement of 8.5 ± 0.2 ppb (using a directly comparable 300 km step model) based on 2016 data falls in the mid-range of the previous measurements, and indicates that the global abundance was not changing substantially in this period.

The vertical profile of propionitrile (as a global average) remains problematic. As pointed out by [Cordiner et al. \(2015\)](#) and also by [Lai et al. \(2017\)](#), photochemical models typically over-estimate the abundance of this gas compared to retrieved abundances (see Fig. 13 (b)), especially in the lower stratosphere, indicating a possible missing loss mechanism. The model which best replicates the data is that of [Willacy et al. \(2016\)](#) (Model C), which includes loss by condensation, sedimentation and haze formation. Despite the abundance at 100–300 km appearing significantly too high, the column abundance of $\sim 10^{14}$ cm^{-2} is of the same order of magnitude as our results. Other models ([Loison et al. 2015](#); [Vuitton et al. 2019](#)) substantially overestimate the column by a factor of ~ 100 , by continuing significant gas mixing fractions down to the tropopause.

REFERENCES

- Ahrens, V., Lewen, F., Takano, S., et al. 2002, *Z. Naturforschung A*, 57, 669
- Baars, J. M. 2002, *IEEE Xplore*
- Balucani, N., Pacifici, L., Skouteris, D., et al. 2019, *Lecture Notes in Computer Science*, 316
- Bell, J. M., Bougher, S. W., Waite, J. H., et al. 2010a, *Journal of Geophysical Research (Planets)*, 115, E12002
- Bell, J. M., Bougher, S. W., Waite, Jr., J. H., et al. 2010b, *Journal of Geophysical Research (Planets)*, 115, 12018
- Bézard, B., Marten, A., & Paubert, G. 1992, *IAUC*
- Bézard, B., Yelle, R. V., & Nixon, C. A. 2014, *Titan*, 158
- Bogey, M., Demuynck, C., & Destombes, J. 1986, *Chemical Physics Letters*, 125, 383
- Borysow, A. 1991, *Icarus*, 92, 273
- Borysow, A., & Frommhold, L. 1986a, *The Astrophysical journal*, 311, 1043
- . 1986b, *The Astrophysical journal*, 303, 495
- . 1986c, *The Astrophysical journal*, 304, 849
- . 1987, *The Astrophysical journal*, 318, 940
- Borysow, A., & Tang, C. 1993, *Icarus*, 105, 175
- Boucher, D., Burie, J., Demaison, J., et al. 1977, *Journal of Molecular Spectroscopy*, 64, 290

- Brauer, C. S., Pearson, J. C., Drouin, B. J., & Yu, S. 2009, *The Astrophysical Journal Supplement Series*, 184, 133
- Broadfoot, A., Sandel, B. R., Shemansky, D., et al. 1981, *Science*, 212, 206
- Canosa, A., Páramo, A., Picard], S. D. L., & Sims, I. R. 2007, *Icarus*, 187, 558
- Canosa, A., Sims, I. R., Travers, D., Smith, I. W. M., & Rowe, B. R. 1997, *Å*, 323, 644
- Cazzoli, G., & Puzzarini, C. 2005, *Journal of Molecular Spectroscopy*, 233, 280
- . 2006, *Journal of Molecular Spectroscopy*, 240, 153
- Cernicharo, J., Gottlieb, C. A., Guelin, M., et al. 1991, *The Astrophysical Journal*, 368, L39
- Charnley, S. B., Kuan, Y.-J., Huang, H.-C., et al. 2005, *Advances in Space Research*, 36, 137
- Cordiner, M. A., Charnley, S. B., Kisiel, Z., McGuire, B. A., & Kuan, Y.-J. 2017, *The Astrophysical Journal*, 850, 187
- Cordiner, M. A., Nixon, C. A., Charnley, S. B., et al. 2018, *The Astrophysical Journal*, 859, L15
- Cordiner, M. A., Teanby, N. A., Nixon, C. A., et al. 2019, *The Astronomical Journal*, 158, 76
- Cordiner, M. A., Palmer, M. Y., Nixon, C. A., et al. 2015, *ApJL*, 800, L14
- Coustenis, A., Salama, A., Schulz, B., et al. 2003, *Icarus*, 161, 383
- Coustenis, A., Salama, A., Lellouch, E., et al. 1998, *Astron. and Astrophys.*, 336, L85
- Cui, J., Yelle, R. V., Vuitton, V., et al. 2009, *Icarus*, 200, 581
- Daly, A. M., Bermúdez, C., López, A., et al. 2013, *The Astrophysical Journal*, 768, 81
- Dobrijevic, M., Hébrard, E., Loison, J., & Hickson, K. 2014, *Icarus*, 228, 324
- Ehrenfreund, P., Boon, J., Commandeur, J., et al. 1995, *Advances in Space Research*, 15, 335
- Flasar, F. M., Kunde, V. G., Achterberg, R. K., et al. 2004, *Nature*, 427, 132
- Fondren, L. D., McLain, J., Jackson, D. M., Adams, N. G., & Babcock, L. M. 2007, *International Journal of Mass Spectrometry*, 265, 60
- Fosse, D., Cernicharo, J., Gerin, M., & Cox, P. 2001, *The Astrophysical Journal*, 552, 168
- Fuchs, U., Brünken, S., Fuchs, G. W., et al. 2004, *Z. Naturforschung A*, 59, 861
- Fulchignoni, M., Ferri, F., Angrilli, F., et al. 2005, *Nature*, 438, 785
- Gillett, F. C. 1975, *The Astrophysical Journal*, 201, L41
- Gillett, F. C., Forrest, W. J., & Merrill, K. M. 1973, *The Astrophysical Journal*, 184, L93
- Goorvitch, D. 1994, *The Astrophysical Journal Supplement Series*, 95, 535
- Guadagnini, R., Schatz, G. C., & Walch, S. P. 1998, *The Journal of Physical Chemistry A*, 102, 5857
- Hanel, R., Conrath, B., Flasar, F. M., et al. 1981, *Science*, 212, 192
- Hartle, R. E., Sittler, E. C., Neubauer, F. M., et al. 2006, *Planet. Space Sci.*, 54, 1211
- Hébrard, E., Dobrijevic, M., Loison, J. C., et al. 2013, *A&A*, 552, A132
- Heineking, N., Dreizler, H., & Schwarz, R. 1986, *Zeitschrift für Naturforschung A*, 41, 1210
- Hörst, S. M. 2017, *Journal of Geophysical Research: Planets*, 122, 432
- Hörst, S. M., Vuitton, V., & Yelle, R. V. 2008, *Journal of Geophysical Research (Planets)*, 113, E10006
- Iino, T., Sagawa, H., & Tsukagoshi, T. 2020, *The Astrophysical Journal*, 890, 95
- Irwin, P. G. J., Teanby, N. A., de Kok, R., et al. 2008, *J. Quant. Spectr. Rad. Trans.*, 109, 1136
- Kanata, H., Yamamoto, S., & Saito, S. 1987, *Chemical Physics Letters*, 140, 221
- Khare, B., Sagan, C., Thompson, W., et al. 1984, *Advances in Space Research*, 4, 59
- Kisiel, Z., Nixon, C. A., Cordiner, M. A., Thelen, A. E., & Charnley, S. B. 2020, *J. Mol. Spectrosc.*, 372
- Kisiel, Z., Pszczółkowski, L., López, J. C., et al. 1999, *Journal of Molecular Spectroscopy*, 195, 332
- Krasnopolsky, V. A. 2009, *Icarus*, 201, 226
- . 2010, *Planet. Space Sci.*, 58, 1507
- Krasnopolsky, V. A. 2012, *Planetary and Space Science*, 73, 318
- . 2014, *Icarus*, 236, 83
- Kuan, Y.-J., Charnley, S. B., Huang, H.-C., et al. 2004, *Advances in Space Research*, 33, 31
- Kuan, Y.-J., Yan, C.-H., Charnley, S. B., et al. 2003, *Monthly Notices of the Royal Astronomical Society*, 345, 650
- Kuiper, G. P. 1944, *ApJ*, 100, 378

- Kukolich, S. G. 1982, *The Journal of Chemical Physics*, 76, 97
- Kukolich, S. G., Ruben, D. J., Wang, J. H. S., & Williams, J. R. 1973, *The Journal of Chemical Physics*, 58, 3155
- Kunde, V. G., Aikin, A. C., Hanel, R. A., et al. 1981, *Nature*, 292, 686
- Lacy, J. H., Richter, M. J., Greathouse, T. K., Jaffe, D. T., & Zhu, Q. 2002, *Publications of the Astronomical Society of the Pacific*, 114, 153
- Lai, J. C.-Y., Cordiner, M. A., Nixon, C. A., et al. 2017, *The Astronomical Journal*, 154, 206
- Lellouch, E. 2007, *Astrophysics and Space Science*, 313, 175
- Loison, J., Hébrard, E., Dobrijevic, M., et al. 2015, *Icarus*, 247, 218
- Lombardo, N. A., Nixon, C. A., Achterberg, R. K., et al. 2019, *Icarus*, 317, 454
- Lovas, F. J. 1992, *Journal of Physical and Chemical Reference Data*, 21, 181
- Lutz, B. L., de Bergh, C., & Owen, T. 1983, *Science*, 220, 1374
- Maguire, W. C., Hanel, R. A., Jennings, D. E., Kunde, V. G., & Samuelson, R. E. 1981, *Nature*, 292, 683
- Maiwald, F., Lewen, F., Ahrens, V., et al. 2000, *Journal of Molecular Spectroscopy*, 202, 166
- Martins, Z. 2018, *Life*, 8, 28
- McGuire, B., Burkhardt, A., Kalenskii, S., et al. 2018, *Science*, 359, 202
- Molter, E. M., Nixon, C. A., Cordiner, M. A., et al. 2016, *The Astronomical Journal*, 152, 42
- Müller, H. S., Belloche, A., Menten, K. M., Comito, C., & Schilke, P. 2008, *Journal of Molecular Spectroscopy*, 251, 319, special issue dedicated to the pioneering work of Drs. Edward A. Cohen and Herbert M. Pickett on spectroscopy relevant to the Earth's atmosphere and astrophysics
- Müller, H. S., Schlöder, F., Stutzki, J., & Winnewisser, G. 2005, *Journal of Molecular Structure*, 742, 215
- Müller, H. S. P., Thorwirth, S., Roth, D. A., & Winnewisser, G. 2001, *Å*, 370, L49
- Niemann, H. B., Atreya, S. K., Bauer, S. J., et al. 2002, *Space Science Reviews*, 104, 553
- Niemann, H. B., Atreya, S. K., Demick, J. E., et al. 2010, *Journal of Geophysical Research (Planets)*, 115, 12006
- Nixon, C. A., Teanby, N. A., Irwin, P., & Hörst, S. M. 2013a, *Icarus*, 224, 253
- Nixon, C. A., Achterberg, R. K., Vinatier, S., et al. 2008, *Icarus*, 195, 778
- Nixon, C. A., Achterberg, R. K., Teanby, N. A., et al. 2010, *Faraday Discussions*, 147, 65
- Nixon, C. A., Temelso, B., Vinatier, S., et al. 2012, *Astrophys. J.*, 749, 159
- Nixon, C. A., Jennings, D. E., Bézard, B., et al. 2013b, *ApJL*, 776, L14
- Nuevo, M., Materese, C. K., & Sandford, S. A. 2014, *The Astrophysical Journal*, 793, 125
- Palmer, M. Y., Cordiner, M. A., Nixon, C. A., et al. 2017, *Science Advances*, 3, e1700022
- Peeters, Z., Botta, O., Charney, S. B., et al. 2005, *Å*, 433, 583
- Pickett, H. M., Poynter, R. L., Cohen, E. A., et al. 1998, *Journal of Quantitative Spectroscopy and Radiative Transfer*, 60, 883
- Rodgers, C. D. 2000, *Series on Atmospheric, Oceanic and Planetary Physics*, doi:10.1142/3171
- Samuelson, R. E., Hanel, R. A., Kunde, V. G., & Maguire, W. C. 1981, *Nature*, 292, 688
- Samuelson, R. E., Maguire, W. C., Hanel, R. A., et al. 1983, *J. Geophys. Res.*, 88, 8709
- Schinder, P. J., Flasar, F. M., Marouf, E. A., et al. 2012, *Icarus*, 221, 1020
- Serigano, J., Nixon, C. A., Cordiner, M. A., et al. 2016, *The Astrophysical Journal*, 821, L8
- Simon, M. N., & Simon, M. 1973, *The Astrophysical Journal*, 184, 757
- Soorkia, S., Taatjes, C. A., Osborn, D. L., et al. 2010, *Physical Chemistry Chemical Physics*, 12, 8750
- Stoks, P. G., & Schwartz, A. W. 1982, *Geochimica et Cosmochimica Acta*, 46, 309
- Teanby, N., Irwin, P., Nixon, C., et al. 2013, *Planetary and Space Science*, 75, 136
- Teanby, N. A., Irwin, P. G. J., de Kok, R., et al. 2009, *Icarus*, 202, 620
- Teanby, N. A., Cordiner, M. A., Nixon, C. A., et al. 2018, *The Astronomical Journal*, 155, 251
- Thaddeus, P., Vrtilik, J. M., & Gottlieb, C. A. 1985, *The Astrophysical Journal*, 299, L63
- Thelen, A. E., Nixon, C. A., Cordiner, M. A., et al. 2019a, *The Astronomical Journal*, 157, 219
- Thelen, A. E., Nixon, C., Chanover, N., et al. 2018, *Icarus*, 307, 380

- . 2019b, *Icarus*, 319, 417
- Vrtilek, J. M., Gottlieb, C. A., & Thaddeus, P. 1987, *The Astrophysical Journal*, 314, 716
- Vuitton, V., Yelle, R. V., & Anicich (Retired), V. G. 2006, *The Astrophysical Journal*, 647, L175
- Vuitton, V., Yelle, R. V., Klippenstein, S. J., Hörst, S. M., & Lavvas, P. 2019, *Icarus*
- Vuitton, V., Yelle, R. V., & Lavvas, P. 2009, *Royal Society of London Philosophical Transactions Series A*, 367, 729
- Vuitton, V., Yelle, R. V., & McEwan, M. J. 2007, *Icarus*, 191, 722
- Waite, J. H., Lewis, W. S., Kasprzak, W. T., et al. 2004, *SSRv*, 114, 113
- Waite, J. H., Niemann, H., Yelle, R. V., et al. 2005, *Science*, 308, 982
- Walch, S. P. 1995, *The Journal of Chemical Physics*, 103, 7064
- Westlake, J. H., Bell, J. M., Waite, Jr., J. H., et al. 2011, *Journal of Geophysical Research (Space Physics)*, 116, A03318
- Willacy, K., Allen, M., & Yung, Y. 2016, *The Astrophysical Journal*, 829, 79
- Wilson, E. H., & Atreya, S. K. 2004, *Journal of Geophysical Research (Planets)*, 109, 6002
- Winnewisser, G., Belov, S., Klaus, T., & Schieder, R. 1997, *Journal of Molecular Spectroscopy*, 184, 468
- Wlodarczak, G., Martinache, L., Demaison, J., & Van Eijck, B. P. 1988, *Journal of Molecular Spectroscopy*, 127, 200
- Young, D. T., Berthelier, J. J., Blanc, M., et al. 2004, *Space Science Reviews*, 114, 1